This Accepted Manuscript has not been copyedited and formatted. The final version may differ from this version.

JNeurosci
THE JOURNAL OF NEUROSCIENCE

Research Articles: Development/Plasticity/Repair

Developmental disruption of recurrent inhibitory feedback results in compensatory adaptation in the Renshaw cell - motor neuron circuit

Anders Enjin[1], Sharn Perry[1], Markus M Hilscher, Chetan Nagaraja, Martin Larhammar, Henrik Gezelius, Anders Eriksson, Katarina E Leão and Klas Kullander

Department of Neuroscience, Uppsala University, Box 593, 751 24, Uppsala, Sweden

DOI: 10.1523/JNEUROSCI.0949-16.2017

Received: 22 March 2016

Revised: 6 April 2017

Accepted: 25 April 2017

Published: 8 May 2017

Author contributions: KK and AE conceived the study. HG generated the *Chrna2Cre* mouse line. AE performed and analyzed molecular, extracellular electrophysiology and behavior experiments. CN performed and analyzed stretch reflex experiments. SP, MH and KEL performed and analyzed patch-clamp electrophysiology recordings. AEr and ML performed and analyzed molecular experiments and treadscan data. SP, AE and KK wrote the manuscript.

This work was financed by grants from the Swedish Medical Research Council, Hållsten, Ländells, the Swedish Brain Foundation, the Swedish Foundation for Cooperation in Research and Higher Education, and CNPq-Brasil. AE present address: Department of Biology, Lund University, Naturvetarvägen 2, 223 62 Lund, Sweden. ML present address: Department of Neuroscience, Genentech Inc., South San Francisco, CA 94080, USA, KEL present address: Brain Institute, Federal University of Rio Grande do Norte, Natal, Brazil. The authors declare no competing financial interests.

[1]These authors contributed equally to this work

Correspondence: Klas Kullander, Uppsala University, Box 593, 751 24, Uppsala Sweden, Fax: +46184714172, Email: klas.kullander@neuro.uu.se

Cite as: J. Neurosci ; 10.1523/JNEUROSCI.0949-16.2017

Alerts: Sign up at www.jneurosci.org/cgi/alerts to receive customized email alerts when the fully formatted version of this article is published.

Accepted manuscripts are peer-reviewed but have not been through the copyediting, formatting, or proofreading process.

Copyright © 2017 the authors

JNeurosci Accepted Manuscript

JNeurosci Accepted Manuscript

Developmental disruption of recurrent inhibitory feedback results in compensatory adaptation in the Renshaw cell - motor neuron circuit

Anders Enjin[1], Sharn Perry[1], Markus M Hilscher, Chetan Nagaraja, Martin Larhammar, Henrik Gezelius, Anders Eriksson, Katarina E Leão, Klas Kullander*

Department of Neuroscience, Uppsala University, Box 593, 751 24, Uppsala, Sweden

[1] These authors contributed equally to this work

* Correspondence:

Klas Kullander, Uppsala University, Box 593, 751 24, Uppsala Sweden

Fax: +46184714172

Email: klas.kullander@neuro.uu.se

Abbreviated title: Loss of VIAAT mediated signaling in Renshaw cells

Number of Pages: 47

Figures: 7

Tables: 2

Words: Abstract; 201, Introduction; 388, Discussion; 1359

Keywords: Spinal cord, Interneurons, Nicotinic acetylcholine receptor alpha2, mouse, VIAAT, VGAT, ChAT

Author contributions: KK and AE conceived the study. HG generated the *Chrna2*^{Cre} mouse line. AE performed and analyzed molecular, extracellular electrophysiology and behavior experiments. CN performed and analyzed stretch reflex experiments. SP, MH and KEL performed and analyzed patch-clamp electrophysiology recordings. AEr and ML performed and analyzed molecular experiments and treadscan data. SP, AE and KK wrote the manuscript.

JNeurosci Accepted Manuscript

Acknowledgements:

This work was financed by grants from the Swedish Medical Research Council, Hållsten, Ländells, the Swedish Brain Foundation, the Swedish Foundation for Cooperation in Research and Higher Education, and CNPq-Brasil. AE present address: Department of Biology, Lund University, Naturvetarvägen 2, 223 62 Lund, Sweden. ML present address: Department of Neuroscience, Genentech Inc., South San Francisco, CA 94080, USA, KEL present address: Brain Institute, Federal University of Rio Grande do Norte, Natal, Brazil. The authors declare no competing financial interests.

JNeurosci Accepted Manuscript

Abstract

When activating muscles, motor neurons in the spinal cord also activate Renshaw cells, which provide recurrent inhibitory feedback to the motor neurons. The tight coupling with motor neurons suggests that Renshaw cells have an integral role in movement, a role that is yet to be elucidated. Here we used the selective expression of the nicotinic cholinergic receptor alpha 2 (*Chrna2*) in mice to genetically target the vesicular inhibitory amino acid transporter (VIAAT) in Renshaw cells. Loss of VIAAT from *Chrna2*^{Cre} expressing Renshaw cells did not impact any aspect of drug-induced fictive locomotion in the neonatal mouse, nor did it change gait, motor coordination or grip strength in adult mice of both sexes. However, motor neurons from neonatal mice lacking VIAAT in Renshaw cells received spontaneous inhibitory synaptic input with a reduced frequency, showed lower input resistance and had an increased number of proprioceptive glutamatergic and calbindin labeled putative Renshaw cell synapses on their soma and proximal dendrites. Concomitantly, Renshaw cells developed with increased excitability and a normal number of cholinergic motor neuron synapses indicating a compensatory mechanism within the recurrent inhibitory feedback circuit. Our data suggest an integral role for Renshaw cell signaling in shaping the excitability and synaptic input to motor neurons.

JNeurosci Accepted Manuscript

Significance Statement: We here provide a deeper understanding of spinal cord circuit formation and the repercussions for the possible role for Renshaw cells in speed and force control. Our results suggest that while Renshaw cells are not directly required as an integral part of the locomotor coordination machinery, development of their electrophysiological character is dependent on VIAAT mediated signaling. Further, Renshaw cell signaling is closely associated to the molding of motor neuron character proposing the existence of a concerted maturation process, which seems to endow this particular spinal cord circuit with the plasticity to compensate for loss of the Renshaw cell in adult circuit function.

JNeurosci Accepted Manuscript

Introduction

The precise activation of muscles by motor neurons is a core component of movement in vertebrates (Kullander, 2005). In parallel to sending the activating signal to muscles, motor neurons activate inhibitory interneurons called Renshaw cells through axon collaterals. Renshaw cells in turn send a recurrent inhibitory signal to the motor neuron (Renshaw, 1946; Eccles et al., 1954). The close relationship of Renshaw cells with motor neurons through recurrent inhibitory circuits suggests an integral function of Renshaw cells for motor neuron activity, but their specific role for movement remains poorly understood (Windhorst, 1996; Alvarez and Fyffe, 2007;).

In rodents and cats, Renshaw cells are rhythmically active during fictive locomotion (McCrea et al., 1980; Nishimaru et al., 2006). Motor neurons constitute the main source of excitatory inputs to Renshaw cells during locomotor activity and blocking this input with the nicotinic receptor antagonist mecamylamine limits the spiking activity of Renshaw cells (Noga et al., 1987; Nishimaru et al., 2006). Under these conditions, a lowered fictive locomotor frequency in the mouse and an increased number of spikes generated by motor neurons per burst in the cat is observed (Noga et al., 1987; Nishimaru et al., 2006). A similarly reduced locomotor frequency was observed when motor neuron input to Renshaw cells was removed in choline acetyltransferase (ChAT) knockout mice and when the so-called V1 neurons (a diverse population of spinal interneurons that include Renshaw cells) were ablated, both locomotor frequency and motor neuron spiking were affected (Myers et al., 2005; Gosgnach et al., 2006). These studies infer a role for Renshaw cells in the regulation of locomotor frequency and motor neuron spiking, however, the methodologies used affected additional spinal populations. Thus, firm conclusions regarding the specific role of Renshaw cells are therefore difficult to make (Alvarez

JNeurosci Accepted Manuscript

and Fyffe, 2007; Goulding, 2009; Brownstone and Bui, 2010).

To address the particular role of Renshaw cells in the development and function of locomotor circuitry, we used a transgenic mouse that specifically targets Renshaw cells expressing the nicotinergic receptor α2, *Chrna2* (Perry et al., 2015). We crossed the *Chrna2*^{Cre} mouse with a mouse carrying a conditional allele for the transporter essential to load GABA and Glycine into synaptic vesicles, the vesicular inhibitory amino acid transporter (*Slc32a1* encoding VIAAT; Tong et al., 2008) and studied the phenotypic consequences and possible alterations in the motor neuron – Renshaw cell circuit.

JNeurosci Accepted Manuscript

Materials and methods

Mice

Chrna2^{Cre} mice, *Viaat*$^{lx/lx}$ mice and *R26.lsl.tdTomato* mice have been described elsewhere (Tong et al., 2008; Madisen et al., 2010; Leao et al., 2012; Perry et al., 2015). All animal procedures were approved by the appropriate local Swedish ethical committee (permit C248/11) and experiments were carried out in accordance with the Swedish guidelines. Animals of either sex were maintained on a mixed 129/Sv;C57BL/6 background and housed under the approval of the animal care facility of Uppsala University. *Chrna2*^{Cre} negative littermates (*Viaat*$^{lx/lx}$) were used as control animals. Tail tips from newborn mice were routinely collected for DNA extraction followed by genotyping using polymerase chain reaction (PCR).

In situ hybridization and immunofluorescence

In situ hybridization and immunohistochemistry were performed as previously described on lumbar spinal cord tissue from three-week-old mice (Enjin et al., 2010). The *Viaat (SLC32A1)* cRNA probe covered nucleotides 588-2072 (GeneID: 22348/NM_009508.2). The following antibodies were used in the immunohistochemistry procedures: polyclonal goat anti-ChAT (1:100; AB144P, Milipore), polyclonal goat anti-VAChT (vesicular acetylcholine transporter, 1:500, AB1578, Milipore), polyclonal rabbit- and guinea pig anti-Vglut1 (vesicular glutamate transporter 1, both at 1:300, (Fujiyama et al., 2001), polyclonal rabbit anti-Calbindin (1:5000, CB38, Swant), monoclonal mouse anti-VIAAT (1:500, 131 011, Synaptic Systems) and monoclonal mouse anti synaptophysin (1:500, Sigma-Aldrich). Images were captured on a Zeiss LSM Meta 510 confocal microscope and analyzed using ImageJ software.

JNeurosci Accepted Manuscript

Quantification of synapses was performed on 14 µm sections of lumbar spinal cord from three-week-old mice. Only motor neurons located in the lateral motor column (LMC) were analyzed and putative gamma-motor neurons, defined by a small soma area and absence of C-boutons (Kanning et al., 2010) were excluded from analysis. Synapses, defined by the expression of specific synapse markers co-expressed with synaptophysin, located on motor neuron soma and proximal dendrites (up to 20 µm from soma) were manually counted in a z-stack, captured with a 63×, 1.4 numerical aperture objective at a resolution of 1024 × 1024. Quantification of the number of calbindin-expressing cells and co-expression of Calbindin and *Viaat* mRNA was performed on 7 µm z-stacks from lumbar spinal cord.

Electrophysiology

Spinal cord tissue from control ($Viaat^{lx/lx}$) and $Chrna2^{Cre}$;$Viaat^{lx/lx}$ mice (P0-P7) were prepared as previously described (Perry et al., 2015) with modifications to slicing thickness (270-300 µm). Slices were collected from the entire length of the lumbar region and incubated for 45 min-1hr in artificial cerebrospinal fluid (aCSF) containing in mM: (128 NaCl; 4 KCl; 0.5 NaH_2PO_4; 21 $NaHCO_3$; 30 D-glucose; 1.5 $CaCl_2$; 1 $MgSO_4$; equilibrated with 95% O_2 and 5% CO_2) at 35 °C and subsequently held at room temperature (22-24 °C) during electrophysiological recordings. The spinal cord slices were placed into the recording chamber and superfused with oxygenated aCSF at a rate of 2-4 ml/min. Patch electrodes (3-9 MΩ) from borosilicate glass capillaries (GC150F-10, Harvard Apparatus, Holliston, United States) pulled on a PC-10 gravitational pipette puller (Narishige, Japan) contained a K^+ based internal solution (in mM): 130 K-gluconate, 7 NaCl, 10 HEPES, 0.1 EGTA, 0.3 $MgCl_2$, 2 ATP 0.5 GTP, with pH adjusted to 7.2 using KOH with an osmolarity between 280-

JNeurosci Accepted Manuscript

300mOsm/L. The liquid junction potential was calculated as 14.4 mV using Clampex software version 10.2.

Motor neurons, identified by their stereotypical morphology, and Renshaw cells, identified by RFP expression and ventral horn location, were visualized on a BX51WI Olympus microscope fitted with infrared differential interference contrast optics and a Lambda LS Xenon Arc lamp (Sutter instruments, California, United States) for fluorescent light. Ventral roots were positioned into glass suction electrodes and Renshaw cell firing was confirmed through an antidromic response to ventral root stimulation, where stimulation was approximately 1.5x threshold (A360 WPI Stimulus isolator, World Precision Instruments, Sarasota, USA).

Whole-cell current clamp recordings from identified motor neurons and Renshaw cells were made using a Multiclamp 700B or an Axopatch 200B amplifier (Axon Instruments, California, United States) and digitalized with a data acquisition card (National Instruments, Austin, Texas, USA), low pass filtered at 4 or 5 kHz, digitized at 10 kHz, and acquired in WinWCP software (Dr. J. Dempster, University of Strathclyde, Glasgow, UK), Axograph X (Sydney, Australia) and/or Matlab (Mathworks). Electrophysiological data was analyzed in Axograph X or Matlab.

A small hyperpolarizing bias current was used to maintain a resting membrane potential of -60 mV for motor neurons. Renshaw cells were voltage clamped at -60 mV. Motor neurons and Renshaw cells with a stable resting membrane potential (V_m) lower than -45 mV were included in analysis. Action potentials elicited from depolarizing current pulses (5 pA increments, 20 ms) or a suprathreshold current injection (3 nA, 2 ms; (Nakanishi and Whelan, 2010)) from resting potential, were

JNeurosci Accepted Manuscript

analyzed for action potential (AP) and afterhyperpolarisation (AHP) parameters: amplitude, half-width (50% of spike amplitude or 50% of negative peak amplitude from onset baseline), rise (from 10% to 90% of peak), location (time at which peak amplitude occurs) and onset (at 5% of negative peak amplitude). The AHP time to peak was calculated as the location of the peak minus the AHP onset. Rheobase was noted as the minimum depolarizing injected current (Motor neurons; 20 pA increments, 25 ms: Renshaw cells 5 pA increments, 20 ms) sufficient to evoke an action potential. The AP threshold potential was measured from the first AP fired and noted as the point when the increase in potential exceeds >50 mV/ms. Motor neuron input resistance was calculated from the average response to a hyperpolarizing current (-50 pA, 500 ms, 20 repetitions). Depolarizing current steps (-300 to +400 pA, 50 pA increments, 1 s duration) were used to record AP firing frequency (calculated from the last 500 ms of a 1 s current step) and initial doublet distance (400 pA (MN) and 100pA (RC)). The initial (Max) firing frequency (Hz) was defined as the inverse of the first three interspike intervals (ISI) during a 50/100/250 pA current step. The steady state firing frequency (Hz) was defined as the average of the inverse of the last three interspike intervals in a 50/100/250 pA current step. The percentage increase or decrease in Renshaw cell and motor neuron properties from control was calculated by dividing the calculated difference between control and $Chrna2^{Cre};Viaat^{lx/lx}$ values by the control value for each parameter. For recordings of miniature inhibitory postsynaptic currents (mIPSCs) a cesium chloride (in mM: 120 CsCl, 4 NaCl, 4 $MgCl_2$, 0.001 $CaCl_2$, 10 HEPES, 3 Mg-ATP, 0.3 GTP-Tris and 10 EGTA) based internal solution was used, with the chloride reversal potential close to zero (E_{rev} Cl^- -0.6 mV). Tetrodotoxin (TTX; 1 µM, Tocris Bioscience) was routinely added to the aCSF. Free run traces of 60 s were collected using AxoGraph (Axon Instruments) and

JNeurosci Accepted Manuscript

mIPCS were detected based on threshold and waveform using Matlab (version 2013a, MathWorks). The instantaneous frequency (1/interspike intervals), amplitude and rise time of miniature IPSCs were analysed before and after the addition of the $GABA_A$ receptor antagonist picrotoxin (PTX; 10μM, Tocris Bioscience). Sample means are plotted as box plots and reported as mean ± Standard Error of the Mean (SEM). Data larger than q3 + 1.5*(q3 – q1) or smaller than q1 – 1.5*(q3 – q1), with q1 and q3 denoting the 25th and 75th percentiles (see box plots), was considered an outlier and discarded.

Extracellular electrophysiology

P0-P2 (fictive locomotion) or P5-P6 (stretch reflex) mice were anesthetized with isoflurane, decapitated, eviscerated and submerged in ice-cold dissection buffer containing the following (in nM: 128 NaCl, 4.69 KCl, 25 $NaHCO_3$, 1.18 KH_2PO_4, 3.5 $MgSO_4$, 0.25 $CaCl_2$ and 22 D-Glucose; equilibrated with 95% O_2 and 5% CO_2). The spinal cord was carefully dissected out of the spinal column and placed in a Sylgard-coated chamber. Spinal cords for stretch reflex experiments were hemisected along the midline using a tungsten needle. The spinal cord was then left for >15 minutes to recover while the chamber was superfused with aCSF containing the following (in nM: 128 NaCl, 4.69 KCl, 25 $NaHCO_3$, 1.18 KH_2PO_4, 1.25 $MgSO_4$, 2.5 $CaCl_2$ and 22 D-Glucose; equilibrated with 95% O_2 and 5% CO_2).

For stretch reflex experiments, dorsal and ventral lumbar level (L)2 or L3 roots were placed into glass suction electrodes. Dorsal roots were stimulated using a stimulus isolator unit (A365, World precision instruments) with current pulses of increasing intensity (0-30 μA, 0.2 ms pulses), until maximal reflex amplitude was reached.

JNeurosci Accepted Manuscript

During experiments, stimulus intensity was increased to 1.5x the intensity that generated the maximal response (7.5 – 45 μA) and stimulus pulses were given every 30 seconds. For synaptic depression experiments, ten 1.5x intensity pulses were delivered at 1 Hz and 8 Hz. Recordings were made with alternating current (AC) filtered at 0.1 - 1000 Hz, amplified (1000 x) and digitized at 10 kHz with a Digidata 1440A using pClamp 10.2 software (Molecular Devices).

Fictive locomotion experiments were performed as previously described (Rabe et al., 2009; Andersson et al., 2012). Spinal cords were placed in the recording chamber, continually superfused with aCSF and fictive locomotion was induced by addition of N-methyl-D-aspartate (NMDA, 5 μM) + Serotonin (5-HT, 10 μM) to the perfusate (Wegmeyer et al., 2007). For experiments with increasing NMDA concentration 50 μM Dopamine was also included. Recorded compound action potentials were bandpass-filtered (100 – 10,000 Hz) and digitized using Axoscope 8.1 (Axon Instruments Inc.). For mecamylamine experiments, mecamylamine (50 μM) was added in combination with the neurochemicals after 20 minutes of stable locomotion had been recorded. The spinal cord was exposed to mecamylamine for 50 minutes prior to recording. After recording, the spinal cord was perfused with NMDA and 5-HT for 50 minutes before recording the washout traces. There was little or no recovery after washout, as has previously been described (Mentis et al., 2005).

Data analysis

Recordings were analyzed using Clampfit 10.2 (Molecular Devices). Stretch reflex experiments were analyzed offline by averaging 18-20 traces (deviant spontaneous events were excluded from the averages). The latency was defined as the time between stimulus artifact to first deflection in potential (monosynaptic) and second

JNeurosci Accepted Manuscript

deflection potential (polysynaptic). The amplitude was measured as the highest peak following the monosynaptic and polysynaptic deflections. The polysynaptic area was measured from the second deflection and the following 80 ms between the response and baseline. For synaptic depression experiments the maximal monosynaptic amplitude was measured after each stimulus pulse. The monosynaptic amplitudes were normalized relative to the first amplitude.

Fictive locomotion data was analyzed using the Matlab-based programs Spinalcore and Neurodata (Mor and Lev-Tov, 2007; Zhang et al., 2008). For analysis in Spinalcore the data was downsampled to 250 Hz and rectified. A Morlet wavelet transform was used to extract the phase and frequency throughout 300 seconds of data. A continuous band of significant coherence selected for analysis of mean phase, frequency and analysis. For analysis in Neurodata 600 seconds of data was low-pass filtered at 5 Hz, rectified and high-pass filtered at 0.01 Hz. The resulting trace was analyzed for burst, interburst and cycle period duration as described (Zhang et al., 2008).

Behavior

All behaviors were tested on eight control (*Viaat*$^{lx/lx}$) and nine *Chrna2*^{Cre}*; Viaat*$^{lx/lx}$ 8-week-old mice unless otherwise stated. The experiments were designed with a given maximum time for all experiments. If the maximum time was reached, that animal was excluded from the test. The experimenter was blind to genotype while performing and analyzing the experiments.

JNeurosci Accepted Manuscript

Treadmill locomotor experiments were performed and analyzed essentially as described (Andersson et al., 2012). Treadmill locomotion was conducted at 20 cm/s and gait parameters were automatically analyzed using the Treadscan (CleverSys Inc, Reston, Virginia, USA). Outliers and miss-calculated steps recognized by the Treadscan software and were manually removed before statistical comparison.

Accelerating rotarod experiments used a Rotorod device (IITC life science Inc., Woodland Hills, CA) in three trials each separated by at least 10 minutes. The rod accelerated from 0 to 45 rpm during 60 seconds and maintained rotating at maximum speed for another 60 seconds. In most experiments the device semi-automatically recorded the speed at which the mouse fell from the rod. Steady-speed rotarod experiments were tested at 5, 10, 15 and 20 rpm. Mice were placed on a still rotarod and the time they remained on the rotarod while it was moving was recorded. Occasionally a mouse would fall without the sensors detecting it, in which case the experimenter would register the fall manually. The lag in these instances was not more that 1 second, corresponding to 0.75 rotations/min. In some instances a mouse would cling to the rods, spin one rotation and then fall. At this time the experimenter manually recorded the time of the fall after one full rotation.

Beam walking, the ability to cross a 1 meter rounded wooden beam, was tested on 8-week-old mice. First, the mice were given three test trials on a 25 mm diameter rod. For the experiment, the mice were tested on a 12 mm diameter rod. The mice were videotaped from behind and the time to cross the rod was recorded manually. During analysis, the videotape was played in slow motion and the hind paw foot faults of each mouse were counted. A maximum crossing time of 15 seconds was employed to exclude mice that were not directly crossing the beam.

JNeurosci Accepted Manuscript

Ladder walking was performed on an elevated ladder with 30 cm high plastic glass walls and 4 mm metal rungs separated by 1 cm as described in Metz and Whishaw, 2009. Each mouse was given three trials to complete the task. For the second round, 21 of the rungs were removed giving a random spacing (1 and 4 cm) between the rungs. The mice were videotaped from the side during experimentation and foot slips were analyzed in slow motion.

Maximal grip strength was measured using the Bioseb: Grip Strength test (Bio-Gs3, Bioseb, USA). Using their forepaws, mice grasped a wire grid and were pulled back slowly by the experimenter. The force when the mouse released the grid was detected and recorded. Data are presented as the average grip strength across five trials.

Statistical analysis

All statistical analysis was performed using Prism 5.0a (Graphpad) or Matlab (R2013b, Mathworks). Normal distribution was assessed by the Shapiro-Wilk statistical test. The null hypothesis, stating that the population is normally distributed, is accepted when alpha is determined as ≥ 0.05. All behavioral data was analyzed using a Student's unpaired, two-tailed t-Test. All histology data was analyzed using a Mann-Whitney test. Circular statistics and locomotor burst parameters were analyzed as described in (Mor and Lev-Tov, 2007; Zhang et al., 2008). The mecamylamine and increasing NMDA concentration experiments were analyzed using a two-way ANOVA, where the interaction and drug effects were considered significant when $p<0.05$. Active and passive electrophysiological membrane properties, including AP parameters and firing frequency from control and $Chrna2^{Cre}; Viaat^{lx/lx}$ motor neurons and Renshaw cells were analyzed using a student's unpaired, two-tailed t-Test if the data were normally distributed, or the Mann-Whitney test if the data were not

JNeurosci Accepted Manuscript

normally distributed. All histological, electrophysiological and behavioral data represents the mean ± standard error of the mean (SEM) unless otherwise stated. Significance was determined (* $p < 0.05$, ** $p < 0.01$, *** $p < 0.001$).

JNeurosci Accepted Manuscript

Results

Chrna2^{Cre} labels Renshaw cell-derived synapses on motor neurons

For all experiments, we used *Chrna2^{Cre}* mice, which express Cre in defined interneuron populations in the cortex, hippocampus and spinal cord (Leao et al., 2012; Perry et al., 2015). To visualize the genetically targeted *Chrna2* spinal populations, we crossed *Chrna2^{Cre}* mice with the *R26.lsl.tdTomato* line. In the resulting mouse, we found that the large majority (94%) of cells in the ventrolumbar spinal cord that expressed *Chrna2^{Cre}* co-stained with an antibody for the known Renshaw cell marker calbindin (n = 52 cells, 3 mice, P10-P15, see also Perry et al., 2015). *Chrna2^{Cre}; R26.lsl.tdTomato^{+}* boutons that co-stained with calbindin and the vesicular inhibitory amino acid transporter protein (VIAAT) were prominent in the motor neuron region (Fig. 1B). To corroborate that *Chrna2^{Cre}; R26.lsl.tdTomato^{+}* expression was indeed in Renshaw cells, we used antidromic stimulation of ventral roots and simultaneous patching of tomato^{+} neurons. Such stimulation activated a synaptic current in the *Chrna2^{Cre}* cells with a short latency (<2.2 ms), similar to the observed latency of Renshaw cells (Mentis et al., 2006; Perry et al., 2015). Application of the nicotinic antagonist mecamylamine (50 μM) reduced the synaptic current induced in *Chrna2^{Cre}; R26.lsl.tdTomato^{+}* cells upon ventral root stimulation (Fig. 1C; n = 3 cells). Thus, *Chrna2^{Cre}* cells in the spinal cord ventral horn have the hallmark properties of Renshaw cells.

Genetic elimination of Viaat from Renshaw cells alters synaptic inputs on motor neuron soma and proximal dendrite

To explore the contribution of Renshaw cells to the development of motor neurons and motor circuits, we crossed the *Chrna2^{Cre}* mouse to a mouse carrying an allele

JNeurosci Accepted Manuscript

flanking the second exon of *Viaat* with lox sites, for conditional deletion of the *Viaat* gene (Tong et al., 2008). *In situ* hybridization confirmed that *Viaat* mRNA was absent from all calbindin-immunoreactive ventral horn neurons in the lumbar spinal cord of 3-week-old $Chrna2^{Cre};Viaat^{lx/lx}$ mice, whereas in control mice all calbindin-expressing cells co-stained with *Viaat* mRNA (Fig. 2A, control: 22 cells/6 sections/2 cords, $Chrna2^{Cre};Viaat^{lx/lx}$: 105 cells/23 sections/2 cords). The number of calbindin$^+$ cells in the lumbar ventral horn was similar between control and $Chrna2^{Cre};Viaat^{lx/lx}$ mice, suggesting that the elimination of VIAAT has no effect on Renshaw cell survival (control: 3.7 ± 0.67 cells/section, n = 6 sections, $Chrna2^{Cre};Viaat^{lx/lx}$: 4.6 ± 0.60 cells/section, n = 23 sections both from 2 mice, $p = 0.70$). Expression of the Cre protein in mice carrying the $Chrna2^{Cre}$ allele can be detected at embryonic day (E) 12.5 (data not shown), suggesting that in $Chrna2^{Cre};Viaat^{lx/lx}$ mice, the loss of VIAAT activity is initiated early during development. To examine how the absence of VIAAT-mediated Renshaw cell neurotransmission affects the development of recurrent inhibition circuits, we first quantified the number of synapses on both calbindin$^+$ Renshaw cells and ChAT$^+$ motor neurons (Fig. 2B, C). The number of cholinergic contacts (ChAT and VAChT) on calbindin$^+$ Renshaw cells were unchanged in $Chrna2^{Cre};Viaat^{lx/lx}$ mice compared to control mice (Fig. 2B; ChAT$^+$: control: 4.0 ± 0.81, n = 13 Renshaw cells, $Chrna2^{Cre};Viaat^{lx/lx}$: 4.2 ± 1.0, n = 6 Renshaw cells both from 2 mice, $p = 0.85$; VAChT: control: 3.76 ± 0.51, n = 29 Renshaw cells, $Chrna2^{Cre};Viaat^{lx/lx}$: 3.09 ± 0.51, n = 11 Renshaw cells both from 2 mice, $p = 0.68$). Since motor neuron collaterals are the sole cholinergic input to Renshaw cells (Zagoraiou et al., 2009), this suggests that motor neurons do not require Renshaw cell mediated inhibitory feedback (either via GABA or Glycine) to develop synapses onto Renshaw cell soma.

JNeurosci Accepted Manuscript

Next, we looked at the synaptic boutons on lumbar LMC motor neuron soma and proximal dendrite. Motor neurons had an increased number of calbindin^{+}/synaptophysin^{+} contacts on their cell bodies (Fig. 2C; calb^{+}: control: 2.30 ± 0.29, n = 43 motor neurons; *Chrna2^{Cre};Viaat$^{lx/lx}$*: 3.73 ± 0.46, n = 30 motor neurons both from 2 mice, $p = 0.014$), which most likely originate from Renshaw cells or possibly interneurons in the dorsal spinal cord (Geiman et al., 2000). Additionally, glutamatergic input, labeled by the vesicular glutamate transporter 1 (VGLUT1), labeling proprioceptive sensory Ia afferents (Betley et al., 2009), was more abundant on *Chrna2^{Cre};Viaat$^{lx/lx}$* motor neurons when compared to motor neurons in control mice (Fig. 2D, control: 3.39 ± 0.72, n = 13 motor neurons *Chrna2^{Cre};Viaat$^{lx/lx}$*: 7.24 ± 1.06, n = 17 motor neurons both from 2 mice, $p = 0.001$). Lastly, presumable partition cell synapses immunopositive for ChAT (Zagoraiou et al., 2009) were unchanged in *Chrna2^{Cre};Viaat$^{lx/lx}$* mice (Fig. 2C, ChAT^{+}: control: 11.85 ± 0.97, n = 34 motor neurons; *Chrna2^{Cre};Viaat$^{lx/lx}$* : 13.36 ± 1.26, n = 33 motor neurons both from 2 mice, $p = 0.53$). Thus, VIAAT-mediated Renshaw cell signaling influences the development of synapses to motor neurons.

Normal dorsal root-evoked potentials in Chrna2^{Cre};Viaat$^{lx/lx}$ mice

To test if the increased number of excitatory VGLUT1 positive synaptic boutons on motor neurons translate into an altered motor circuit function we exploited the sensory-motor circuit where dorsal root stimulation activates primarily VGLUT1^{+} proprioceptive synapses in the monosynaptic time-window (the stretch reflex). Lumbar level 2 or 3 dorsal roots were stimulated at 1.5X the intensity that generated a maximal response recorded from the corresponding ventral root (Fig. 3A). Despite the increased number of VGLUT1 positive synapses, the monosynaptic response in

JNeurosci Accepted Manuscript

control (n = 12) and *Chrna2*^{Cre}*;Viaat*$^{lx/lx}$ (n = 16) motor neurons had a similar peak amplitude (control:1.70 ± 0. 54 mV; *Chrna2*^{Cre}*; Viaat* $^{lx/lx}$: 1.21 ± 0.24 mV, $p = 0.38$) and latency (control: 4.78 ± 0.21 ms; *Chrna2*^{Cre}*; Viaat* $^{lx/lx}$: 4.82 ± 0.19 ms, $p = 0.90$) (Fig. 3B, C). Likewise, the activated polysynaptic currents (which are not specific to VGLUT1 synapses) were of a similar amplitude *(*control: 0.39 ± 0.073 mV; *Chrna2*^{Cre}*; Viaat* $^{lx/lx}$: 0.45 ± 0.092 mV, $p = 0.67$), latency (control: 11.38 ± 1.13 ms; *Chrna2*^{Cre}*; Viaat* $^{lx/lx}$: 11.79 ± 0.72 ms, $p = 0.76$) and area (control: 13.13 ± 2.60 mV*ms; *Chrna2*^{Cre}*; Viaat* $^{lx/lx}$: 19.90 ± 5.73 mV*ms, $p = 0.42$) in both *Chrna2*^{Cre}*; Viaat*$^{lx/lx}$ and control mice (Fig. 3B, C).

Stimulating dorsal roots with a low frequency (<16 Hz) leads to significant synaptic depression that translates into a reduced evoked amplitude in motor neurons (Li and Burke, 2001). To test whether the increased number of VGLUT1 synapses in *Chrna2*^{Cre}*; Viaat* $^{lx/lx}$ mice might have affected synaptic depression, we stimulated dorsal roots at two low frequencies, 1 Hz and 8 Hz. Both stimuli lead to significant depression of a similar magnitude in both mutant (n = 5) and control mice (n = 6) (Fig. 3D, 1 Hz: Stimulus number $F_{(9, 81)} = 259$, $p < 0.0001$, Interaction, $F_{(9, 81)} = 0.42$, $p = 0.92$; 8 Hz: Stimulus number $F_{(9, 81)} = 288$, $p < 0.0001$, Interaction, $F_{(9, 81)} = 0.19$, $p = 0.99$). Thus, the increased number of VGLUT1^{+} proprioceptive synapses onto motor neurons did not translate into altered motor neuron activation by dorsal root stimulation.

Chrna2^{Cre}*;Viaat*$^{lx/lx}$ *mice performed normally in sensory-motor tests*

Next, we performed a series of motor behavior tests on 8-week-old *Chrna2*^{Cre}*;Viaat*$^{lx/lx}$ (n = 9) and control (n = 8) mice. We found no measureable deficiencies in the forepaw grip strength of *Chrna2*^{Cre}*;Viaat*$^{lx/lx}$ mice (Fig. 3E; control

JNeurosci Accepted Manuscript

133.2 ± 10.5 g, *Chrna2*^{Cre}*;Viaat*^{lxlx} 130.9 ± 8.1 g, $p = 0.84$). Further, we investigated the ability of the mice to maintain balance at different speeds (steady rotarod), their ability to maintain balance as speed increases (accelerating rotarod), and their ability for correct foot placement during a balance act (beam and ladder walking). Motor coordination, both balance and foot placement, was not affected in *Chrna2*^{Cre}*;Viaat*$^{lx/lx}$ mice when compared with controls (Fig. 3F - H: steady rotarod at 5 (control 51.0 ± 4.4 s, *Chrna2*^{Cre}*;Viaat*^{lxlx} 49.3 ± 6.0 s, $p = 0.82$), 10 (control: 34.2 ± 6.5 s, *Chrna2*^{Cre}*;Viaat*^{lxlx}: 40.6 ± 5.7 s, $p = 0.47$), 15 (control: 20.6 ± 7.1 s, *Chrna2*^{Cre}*;Viaat*^{lxlx}: 28.4 ± 7.4 s, $p = 0.46$) and 20 (control: 9.3 ± 2.5 s, *Chrna2*^{Cre}*;Viaat*^{lxlx}: 15.6 ± 3.7 s, $p = 0.19$) rpm; accelerating rotarod control: 18.4 ± 1.1 rpm, *Chrna2*^{Cre}*;Viaat*^{lxlx}: 18.5 ± 1.4 rpm, $p = 0.93$; beam walk foot slips control: 0.3 ± 0.1 slips, *Chrna2*^{Cre}*;Viaat*^{lxlx}: 0.4 ± 0.1 slips, $p = 0.67$, time control: 10.1 ± 1.4 s, *Chrna2*^{Cre}*;Viaat*^{lxlx}: 10.7 ± 2.0 s, $p = 0.82$). The number of foot slips (control: 0.9 ± 0.3 slips, *Chrna2*^{Cre}*;Viaat*^{lxlx}: 2.2 ± 0.7 slips, $p = 0.13$) and the time to cross (control: 37.1 ± 10.5 s, *Chrna2*^{Cre}*;Viaat*^{lxlx}: 51.3 ± 11.4 s, $p = 0.39$) a one meter ladder with random distances between rungs were similar between *Chrna2*^{Cre}*;Viaat*^{lxlx} and control mice (Fig. 3H). Thus, VIAAT-mediated Renshaw cell signaling appears dispensable for the development of normal coordination and maximal strength.

The effects of VIAAT-mediated Renshaw cell signaling on motor behavior

To determine if the absence of VIAAT-mediated Renshaw cell signaling during development alters locomotor behavior in these mice, we performed a detailed analysis of gait. *Chrna2*^{Cre}*; Viaat*$^{lx/lx}$ (n = 9) and control (n = 8) mice were placed to run on a clear treadmill at 20 cm/s while being video taped from underneath. Paw contact to the treadmill and the subsequent gait parameters (stride length, stride

JNeurosci Accepted Manuscript

frequency, swing and stance) were semi-automatically analyzed for locomotor behavior (Table 1). All gait parameters were normal in both control and *Chrna2*^{Cre}; *Viaat*$^{lx/lx}$ mice suggesting that the absence of Viaat-mediated Renshaw cell signaling did not affect the development of the neural circuitry required for the maintenance of normal gait.

Fictive locomotion is normal in the absence of VIAAT-mediated Renshaw cell signaling

The activation of isolated spinal cord central pattern generator (CPG) networks induces a stereotypical pattern of motor activation that generates rhythmic locomotor-like activity in the absence of sensory and supraspinal inputs. To determine if the intrinsic pattern of locomotion was affected by a loss of Renshaw cell VIAAT-mediated inhibition, we measured locomotor-like activity through the spinal cord ventral roots at lumbar segments (L)2 (flexion) and L5 (extension). Drug-induced locomotion (5 µM NMDA and 10 µM 5-HT) induced a stable rhythm in both control and *Chrna2*^{Cre}; *Viaat*$^{lx/lx}$ spinal cords (Fig. 4A, control n = 6; *Chrna2*^{Cre}; *Viaat*$^{lx/lx}$ n = 5). The average frequency of fictive locomotor activity was similar in control and *Chrna2*^{Cre};*Viaat*$^{lx/lx}$ mice where a coherency region emerged at 0.4 Hz for both genotypes (Fig. 4B - E, Frequency: l/r : control: 0.44 ± 0.028 Hz; *Chrna2*^{Cre}; *Viaat* $^{lx/lx}$: 0.41 ± 0.027 Hz, $p = 0.63$, f/e control: 0.48 ± 0.052 Hz; *Chrna2*^{Cre}; *Viaat* $^{lx/lx}$: 0.43 ± 0.087 Hz, $p = 0.61$; Coherence: l/r control: 0.87 ± 0.012; *Chrna2*^{Cre}; *Viaat* $^{lx/lx}$: 0.88 ± 0.0098, $p = 0.47$, f/e control: 0.86 ± 0.019; *Chrna2*^{Cre}; *Viaat* $^{lx/lx}$: 0.84 ± 0.014, $p =$ 0.41). At this frequency, normal L2 left/right alternation activity and flexion-extension (L2 vs. L5) coordination was observed in both control and *Chrna2*^{Cre};*Viaat*$^{lx/lx}$ cords (Fig. 4C). To extend our analysis of the locomotor cycle, we

JNeurosci Accepted Manuscript

applied a time-series algorithm to look at the individual bursts from the L2 segment. In accordance with the other parameters of fictive locomotion, there was no difference in the average cycle period (control: 2.44 ± 0.16 s; *Chrna2*^{Cre}*; Viaat*$^{lx/lx}$: 2.56 ± 0.19 s, $p = 0.66$), burst duration (control: 1.16 ± 0.063 s; *Chrna2*^{Cre}*; Viaat*$^{lx/lx}$: 1.19 ± 0.064 s, $p = 0.73$) or interburst duration (control: 1.28 ± 0.097 s; *Chrna2*^{Cre}*; Viaat*$^{lx/lx}$: 1.34 ± 0.11 s, $p = 0.69$) between control and *Chrna2*^{Cre}*; Viaat*$^{lx/lx}$ mice (Fig. 4F). Additionally, the stability of these parameters was consistent cycle-to-cycle as the coefficient of variation (CoV) was unchanged in the *Chrna2*^{Cre}*; Viaat*$^{lx/lx}$ mutant (Fig. 4G; cycle period control: 0.065 ± 0.0065; *Chrna2*^{Cre}*; Viaat*$^{lx/lx}$: 0.11 ± 0.020, $p = 0.10$, burst duration control: 0.052 ± 0.0052; *Chrna2*^{Cre}*; Viaat*$^{lx/lx}$: 0.066 ± 0.0086, $p = 0.22$, interburst duration, control: 0.10 ± 0.012; *Chrna2*^{Cre}*; Viaat*$^{lx/lx}$: 0.15 ± 0.033, $p = 0.22$). Altogether, this suggests that CPG circuits remain activated in *Chrna2*^{Cre}*; Viaat*$^{lx/lx}$ mice and maintain a rhythmic bursting similar to controls.

The effect of mecamylamine on locomotor frequency during fictive locomotion is not attributable to Renshaw cells

Even if the baseline parameters of fictive locomotion were normal in *Chrna2*^{Cre}*; Viaat*$^{lx/lx}$ mice, it remained possible that provocation of the CPG circuit would uncover a contribution from Renshaw cells to fictive locomotion. Since the nicotinic antagonist mecamylamine lowers the fictive locomotor frequency and blocks the activity of Renshaw cells in fictive locomotion (Nishimaru et al., 2006), we hypothesized that the addition of mecamylamine should not affect the frequency of the locomotor rhythm in *Chrna2*^{Cre}*; Viaat*$^{lx/lx}$ mice. Surprisingly, application of mecamylamine reduced the locomotor frequency in *Chrna2*^{Cre}*; Viaat*$^{lx/lx}$ mice (n = 9) by a similar magnitude to control cords (n = 8) (Fig. 5A-D, Frequency:

JNeurosci Accepted Manuscript

514 mecamylamine $F_{(1, 15)} = 29$ $p < 0.0001$, Interaction, $F_{(1, 15)} = 1.1$, $p = 0.31$; Coherence:
515 mecamylamine $F_{(1, 15)} = 5.4$, $p = 0.03$, Interaction, $F_{(1, 15)} = 0.020$, $p = 0.89$). This
516 slower frequency was attributed to the burst duration (mecamylamine $F_{(1, 15)} = 27$, $p =$
517 0.0001, Interaction, $F_{(1, 15)} = 0.28$, $p = 0.60$), interburst duration (mecamylamine $F_{(1, 15)}$
518 $= 18$ $p = 0.0008$, Interaction, $F_{(1, 15)} = 0.0028$, $p = 0.96$) and cycle period
519 (Mecamylamine $F_{(1, 15)} = 21$, $p = 0.0003$, Interaction, $F_{(1, 15)} = 0.037$, $p = 0.85$) of the
520 locomotor pattern being similarly increased during mecamylamine application in both
521 mutant and control cords (Fig. 5E). The coefficient of variation of these variables was
522 similarly influenced by the application of mecamylamine (Fig. 5E; burst duration
523 (mecamylamine $F_{(1, 15)} = 11$, $p = 0.0051$, interaction, $F_{(1, 15)} = 0.74$, $p = 0.40$),
524 interburst duration (mecamylamine $F_{(1, 15)} = 9.3$ $p = 0.0080$, interaction, $F_{(1, 15)} =$
525 0.0025, $p = 0.96$) and cycle period (mecamylamine $F_{(1, 15)} = 11$, $p = 0.0041$,
526 Interaction, $F_{(1, 15)} = 0.083$, $p = 0.78$)). Thus, the effect of mecamylamine on fictive
527 locomotion appears to be independent of Renshaw cell function.
528 To further probe for a possible function of Renshaw cells during fictive
529 locomotion, we tested increasing excitation levels to mimic increased locomotor
530 speed. To achieve this, we exposed the isolated spinal cords from *Chrna2*^{Cre}*; Viaat*$^{lx/lx}$
531 (n = 6) and age matched control (n = 5) mice, to 10 µM 5-HT and 50 µM dopamine
532 followed by increasing concentrations of NMDA (3 µM and 6 µM). Addition of
533 NMDA similarly increased the frequency of the locomotor cycle in both genotypes
534 (Fig. 5F, frequency: concentration $F_{(2, 16)} = 5.0$, $p = 0.02$, interaction, $F_{(2, 16)} = 0.53$, p
535 $= 0.60$; coherence: concentration $F_{(2, 16)} = 4.2$, $p = 0.04$, interaction, $F_{(2, 16)} = 1.31$, $p =$
536 0.30). This faster frequency in response to increasing NMDA concentrations was
537 caused by a shortening of the burst duration, interburst duration and cycle period in
538 control and *Chrna2*^{Cre}*;Viaat*$^{lx/lx}$ mice, while the coefficient of variation for each

JNeurosci Accepted Manuscript

parameter remained unaffected (Fig. 5G-I, burst duration: concentration $F_{(2, 16)} = 15.7$, $p = 0.0002$, interaction, $F_{(2, 16)} = 0.69$, $p = 0.52$; burst duration CoV: concentration $F_{(2, 16)} = 1.4$, $p = 0.27$, interaction, $F_{(2, 16)} = 0.78$, $p = 0.48$; interburst duration: concentration $F_{(2, 16)} = 9.3$, $p = 0.002$, interaction, $F_{(2, 16)} = 0.21$, $p = 0.81$; interburst duration CoV: concentration $F_{(2, 16)} = 3.0$, $p = 0.08$, interaction, $F_{(2, 16)} = 1.60$, $p = 0.23$; cycle period: concentration $F_{(2, 16)} = 13.2$, $p = 0.0004$, interaction, $F_{(2, 16)} = 0.23$, $p = 0.80$; cycle period CoV: concentration $F_{(2, 16)} = 2.9$, $p = 0.09$, interaction, $F_{(2, 16)} = 1.08$, $p = 0.36$). Thus, we found no evidence that the formation of a functional CPG, including the induction, coordination and stability of the basic fictive locomotor rhythm, required VIAAT-mediated Renshaw cell signaling.

Motor neurons receive a lower frequency of mIPCSs during the first postnatal days in $Chrna2^{Cre}$; $Viaat^{lx/lx}$ mice

To examine if lack of VIAAT-mediated Renshaw cell signaling onto motor neurons was noticeable in the general spontaneous inhibitory release, we recorded miniature inhibitory synaptic currents (mIPSCs) using whole-cell patch clamp, in slices from control ($Viaat^{lx/lx}$, postnatal age 2.4 ± 0.4 days, n = 7) and $Chrna2^{Cre}$; $Viaat^{lx/lx}$, (postnatal age 1.7 ± 0.6 days, n = 7) mice in the presence of TTX (1 μM) (Fig. 6). Traces containing miniature synaptic currents were analysed pairwise before and after addition of PTX (10μM). We measured a significantly lower instantaneous mIPSC frequency from motor neurons in slices where Renshaw cells lacked VIAAT compared to control littermates (Fig. 6B, C; control: 8.85 ± 1.15 Hz; ± $Chrna2^{Cre}$; $Viaat^{lx/lx}$: 5.56 ± 0.72 Hz, $p = 0.032$). No statistical difference in instantaneous mIPSC frequency was seen following application of the $GABA_A$ receptor antagonist PTX (Fig. 6B, C; control: 8.33 ± 1.39 Hz; ± $Chrna2^{Cre}$; $Viaat^{lx/lx}$: 5.09 ± 1.95 Hz, $p = 0.21$)

JNeurosci Accepted Manuscript

indicating that the difference in frequency relies on the glycinergic component of mIPSCs. We did not detect a difference in the average amplitude of mIPSCs (control: 78.29 ± 10.92 pA; ± *Chrna2*^{Cre}*; Viaat*$^{lx/lx}$: 61,44 ± 7.02 pA, $p = 0.22$) or after application of PTX (Fig. 6D, E; control: 52.11 ± 9.61 pA; ± *Chrna2*^{Cre}*; Viaat*$^{lx/lx}$: 63.97 ± 6.68 pA, $p = 0.3354$). However, the mean mIPSC rise time was slower in *Chrna2*^{Cre}*; Viaat*$^{lx/lx}$ mice compared to control littermates (Fig. 6F; control: 3.53 ± 0.12 ms; ± *Chrna2*^{Cre}*; Viaat*$^{lx/lx}$: 4.06 ± 0.14 ms, $p = 0.013$). The application of PTX removed this difference in average rise time (control: 3.32 ± 0.02 ms; ± *Chrna2*^{Cre}*; Viaat*$^{lx/lx}$: 3.34 ± 0.02 ms, $p = 0.36$) indicating that the remaining glycinergic component of mIPSCs, with a faster rise time (compared to the average rise time when GABAergic and glycinergic mIPSCs are mixed), is not different between control and animals lacking VIAAT in Renshaw cells (Fig. 6F). Therefore, loss of Renshaw cell inhibition onto motor neurons (P0-P3) resulted in a reduced frequency of inhibitory spontaneous release, and with a component of $GABA_A$ receptor mediated signaling affecting rise time.

Impact of Renshaw cells on the development of motor neuron electrical properties

To examine if VIAAT-mediated Renshaw cell signaling affects the development of motor neuron intrinsic properties, we performed whole cell patch-clamp experiments from motor neurons in transverse slices from P0-P3 *Chrna2*^{Cre}*; Viaat*$^{lx/lx}$ mice (n = 13) and compared that to age matched control mice (*Viaat*$^{lx/lx}$, n = 9). There was no difference in the membrane potential of motor neurons between control (-54.9 ± 1.9 mV) and *Chrna2*^{Cre}*; Viaat*$^{lx/lx}$ (-54.6 ± 3.4 mV) mice, but there was a significant difference in input resistance (control: 119.5 ± 17.4 MΩ; *Chrna2*^{Cre}*; Viaat*$^{lx/lx}$: 60.1 ± 5.3 MΩ, $p = 0.012$). Motor neurons from *Chrna2*^{Cre}*; Viaat*$^{lx/}$ mice were notably less

JNeurosci Accepted Manuscript

589 excitable, although there was no significant difference in the average action potential
590 threshold (control: -22.2 ± 2.5 mV; *Chrna2*^{Cre}*; Viaat*$^{lx/lx}$ -17.3 ± 3.3 mV; $p = 0.247$).
591 Further, we found no significant differences in average rheobase current, action
592 potential amplitude or half-width (Table 2). The membrane afterhyperpolarization
593 (AHP) was altered, where *Chrna2*^{Cre}*; Viaat*$^{lx/lx}$ motor neurons showed a faster AHP
594 onset and shorter duration compared with controls (Fig. 7A, Table 2, AHP rise:
595 control: 20.9 ± 1.9 ms; *Chrna2*^{Cre}*; Viaat*$^{lx/lx}$: 13.6 ± 0.5 ms, $p = 0.013$. AHP location:
596 control: 134.6 ± 10.0 ms; *Chrna2*^{Cre}*; Viaat*$^{lx/lx}$: 97.2 ± 3.8 ms, $p = 0.016$. AHP onset:
597 control: 97.0 ± 7.3 ms; *Chrna2*^{Cre}*; Viaat*$^{lx/lx}$: 72.0 ± 2.8, $p = 0.027$. AHP time to peak:
598 control: 37.7 ± 4.0 ms; *Chrna2*^{Cre}*; Viaat*$^{lx/lx}$: 25.2 ± 1.5 ms, $p = 0.040$). Other AHP
599 parameters including amplitude and half-width, were not different between genotypes
600 (Table 2). Thus, due to the lower input resistance, *Chrna2*^{Cre}*; Viaat*$^{lx/lx}$ motor neurons
601 required more current input to generate sufficient depolarization to reach action
602 potential threshold.

603 Although requiring more depolarizing current to achieve action potentials, a
604 faster repolarization from hyperpolarized potentials (as seen with the AHP
605 quantification) may allow *Chrna2*^{Cre}*; Viaat*$^{lx/lx}$ motor neurons to readily return to
606 resting membrane potential and thus still be able to follow high firing frequencies
607 when excited by sufficient input to reach threshold. We sought to elucidate the steady
608 state firing frequency of motor neurons in response to depolarization, however, due to
609 the variability in the low input resistance of *Chrna2*^{Cre}*; Viaat*$^{lx/lx}$ motor neurons, a
610 variable amount of current needed to be injected to generate spike trains. To initially
611 elucidate the motor neuron average firing frequency, we grouped their firing
612 responses over two defined current blocks for control and *Chrna2*^{Cre}*; Viaat*$^{lx/lx}$ mice
613 (Fig. 7B inset; control; block A: 0 - 800 pA and C: 850 – 1900 pA: *Chrna2*^{Cre}*;*

JNeurosci Accepted Manuscript

614 *Viaat*$^{lx/lx}$ block B: 0 – 1250 pA, and D: 1300 – 3500 pA). Motor neuron firing
615 frequency was similar in response to low and high current injection for both
616 genotypes (control A: 12.5 ± 1.0 Hz, C: 12.2 ± 0.8 Hz; *Chrna2*^{Cre}*; Viaat*$^{lx/lx}$ B: 9.3 ±
617 0.4 Hz, D: 10.3 ± 0.5 Hz) but *Chrna2*^{Cre}*; Viaat*$^{lx/lx}$ motor neurons fired significantly
618 slower than control neurons at lower current inputs (Fig. 7B; control A: 12.5 ± 1.0 Hz;
619 *Chrna2*^{Cre}*; Viaat*$^{lx/lx}$ B: 9.3 ± 0.4 Hz, $p = 0.003$). As such we compared the slope of
620 the frequency-current gain (Hz/pA) in response to increased current injections instead
621 of a comparison of the firing frequency at a specific current step. We found no
622 significant difference in slope between control and *Chrna2*^{Cre}*; Viaat*$^{lx/lx}$ motor neurons
623 (Fig. 7B; control: 0.0195 ± 0.003 Hz/pA, n = 12; *Chrna2*^{Cre}*; Viaat*$^{lx/lx}$ 0.0125 ± 0.0029
624 Hz/pA, n = 6, $p = 0.151$).
625
626 *Impact of the loss of Renshaw cell VIAAT-mediated signaling on the Renshaw cell*
627 *itself*
628 To determine if VIAAT-mediated Renshaw cell signaling affected the
629 electrophysiological development of the Renshaw cell population, we performed
630 patch-clamp experiments from Renshaw cells in transverse slices from P1-P6
631 *Chrna2*^{Cre}*;Viaat*^{lxlx} mice (n = 13) and compared them to age-matched control mice (n
632 = 13). Passive and active firing properties were examined in a whole-cell current
633 clamp configuration at rest. The *Chrna2*^{Cre}*;Viaat*^{lxlx} Renshaw cells had a more
634 depolarized resting membrane potential (control; -51.6 ± 0.8 mV, *Chrna2*^{Cre}*;Viaat*^{lxlx};
635 -48.2 ± 1.3 mV, $p = 0.002$) and markedly higher input resistances than control
636 neurons (control: 282.0 ± 31.2 MΩ, *Chrna2*^{Cre}*;Viaat*^{lxlx}: 423.7 ± 36.6 MΩ; $p =$
637 0.0071). Stepwise injections of depolarizing current (20 ms, 5 pA increments)
638 generated action potentials in Renshaw cells from both *Chrna2*^{Cre}*;Viaat*^{lxlx} and

JNeurosci Accepted Manuscript

control mice (Fig. 7A), where differences in the action potential shape were apparent. The action potential threshold was more hyperpolarized (control: -30.3 ± 1.3 mV, *Chrna2*^{Cre}*;Viaat*^{lxlx}: -38. 4 ± 1.3 mV, $p = 0.0003$), which coincided with a significantly reduced rheobase current (control 56.1 ± 4.9 pA, *Chrna2*^{Cre}*;Viaat*^{lxlx} 39.6 ± 6.7 pA, $p = 0.05$) in *Chrna2*^{Cre}*;Viaat*^{lxlx} Renshaw cells (Fig. 7A, Table 2). Like the motor neurons, the AP amplitude was similar between genotypes, however the AP half-width was significantly wider in *Chrna2*^{Cre}*;Viaat*^{lxlx} Renshaw cells (Fig. 7A, Table 2, control: 2.2 ± 0.2 ms; *Chrna2*^{Cre}*;Viaat*^{lxlx} : 3.0 ± 0.3 ms, $p = 0.023$). Action potentials from both control and *Chrna2*^{Cre}*;Viaat*^{lxlx} Renshaw cells repolarized with afterhyperpolarisation potentials of similar amplitudes (control; -9.4 ± 0.8 mV, *Chrna2*^{Cre}*;Viaat*^{lxlx} -9.4 ± 0.7 mV, $p = 0.98$), however, *Chrna2*^{Cre}*;Viaat*^{lxlx} Renshaw cell AHPs had a slower onset and longer duration compared to control neurons (Fig. 7A, Table 2, AHP rise: control: 12.3 ± 0.9 ms, *Chrna2*^{Cre}*;Viaat*^{lxlx}: 17.8 ± 1.9 ms; $p = 0.014$, AHP half-width: control: 63.1 ± 5.7 ms, *Chrna2*^{Cre}*;Viaat*^{lxlx}: 97.8 ± 13.4 ms, $p = 0.022$, AHP Location: control: 148.8 ± 2.5 ms; *Chrna2*^{Cre}*;Viaat*^{lxlx}: 159.1 ± 4.2 ms, $p = 0.046$). Thus, *Chrna2*^{Cre}*;Viaat*^{lxlx} Renshaw cells are hyperexcitable and require less depolarizing input to reach the threshold for generating an action potential.

Renshaw cells elicited tonically firing trains of action potentials, triggered by depolarizing current steps (0 – 250 pA, 50 pA increments, 2 s duration). Loss of VIAAT-mediated signaling affected the frequency at which Renshaw cells responded to increasing depolarization as *Chrna2*^{Cre}*;Viaat*^{lxlx} Renshaw cells fired action potentials at a slower frequency than controls (Fig. 7C). This slower firing frequency was maintained across all depolarizing steps (control vs. *Chrna2*^{Cre}*;Viaat*^{lxlx} respectively at 50 pA: 13.6 ± 0.6 Hz, 11.0 ± 0.9 Hz, $p = 0.03$; 100 pA: 19.1 ± 1.3 Hz,

JNeurosci Accepted Manuscript

14.8 ± 1.5 Hz, $p = 0.02$; 150 pA: 24.7 ± 0.7 Hz, 17.6 ± 1.5 Hz, $p = 0.0003$; 200 pA: 26.5 ± 1.3 Hz, 18.3 ± 2.2 Hz, $p = 0.004$; 250 pA: 29.6 ± 1.5 Hz, 21.4 ± 3.0 Hz, $p = 0.02$). This slower firing in *Chrna2*^{Cre}*;Viaat*^{lxlx} mice could be attributed to the slower AHP in *Chrna2*^{Cre}*;Viaat*^{lxlx} Renshaw cells. To further quantify Renshaw cell firing across increasing depolarizing current steps, the firing frequency was extrapolated from the interspike intervals of the first three (max) and the last three (steady state) action potentials in the spike train. A comparison of steady state and maximal firing frequencies revealed that Renshaw cells from both control and *Chrna2*^{Cre}; *Viaat*$^{lx/lx}$ mice adapt their firing frequency similarly over the course of depolarization (data not shown).

To examine changes within the recurrent inhibition circuit, we compared motor neurons and Renshaw cells and their relative changes when VIAAT was deleted (Fig. 7D). Interestingly, in many electrophysiological properties the percentage change of *Chrna2*^{Cre}*;Viaat*^{lxlx} motor neurons was matched by an opposite change in *Chrna2*^{Cre}*;Viaat*^{lxlx} Renshaw cells. Most notably, *Chrna2*^{Cre}*;Viaat*^{lxlx} motor neurons had a 49% decrease in input resistance compared to control, whereas *Chrna2*^{Cre}*;Viaat*^{lxlx} Renshaw cells had a 50% increase in input resistance. Moreover, *Chrna2*^{Cre}*;Viaat*^{lxlx} motor neurons had a 22% and 35% decrease in action potential threshold and AHP rise, respectively; whereas *Chrna2*^{Cre}*;Viaat*^{lxlx} Renshaw cells had a 26% and 44% increase respectively. Thus, significant cellular changes were observed in both motor neurons and Renshaw cells as a consequence of the VIAAT deletion, and in the majority of altered parameters, the changes were reciprocal.

JNeurosci Accepted Manuscript

Discussion

Here we report that the developmental removal of VIAAT-mediated Renshaw cell signaling influences the components, but not the output, of the recurrent inhibition circuit. Renshaw cell function has been tightly linked to motor neuron activity for 60 years but their precise contribution to motor control remains obscure. Our analysis of mice deficient of VIAAT-mediated Renshaw cell signaling suggest that Renshaw cells may be involved in the development of an appropriate response to the synaptic input of motor neurons. Interestingly, the absence of VIAAT-mediated Renshaw cell signaling does not translate to deficient motor behavior or physiological activity in spinal circuits.

Genetic elimination of VIAAT-mediated signaling in Renshaw cells

The subtle phenotypic consequences in *Chrna2*^{Cre}*;Viaat*^{lxlx} mice raised concerns about the efficiency of the VIAAT deletion. We validated that the cre-lox combination used in this study resulted in the removal of *Viaat* mRNA (Fig. 2) and was restricted to *Chrna2* expressing ventral horn populations. VIAAT is the primary vesicular transport protein for inhibitory transmitters and no alternative uptake mechanism for GABA and/or glycine into vesicles is available (Aubrey, 2016; Rahman et al., 2015). Moreover, previous reports demonstrated that genetic deletion of VIAAT resulted in the absence of inhibitory postsynaptic currents (IPSCs) in autaptic cultures (Wojcik et al., 2006) and that *Chrna2*$^{+}$hippocampal interneurons lost their optogenetically induced activity (Leao et al., 2012). When measuring spontaneous inhibitory neurotransmitter release (Fig. 6), we found a lower instantaneous frequency of mIPSCs onto *Chrna2*^{Cre}*;Viaat*^{lxlx} motor neurons, indicative of a reduced spontaneous Renshaw cell-mediated inhibition.

JNeurosci Accepted Manuscript

Motor circuit and motor behavior development in the absence of Renshaw cell signaling

Due to their tight physiological coupling to motor neurons, Renshaw cells have long been thought to play an integral role in the control of locomotion. Here we demonstrate that genetically inactivating Renshaw cell inhibitory neurotransmitter transport did not result in any abnormalities in fictive locomotion or motor behavior. Fictive locomotion parameters including coordination, frequency and burst activity, and the cycle-to-cycle variation in these parameters were not changed in *Chrna2*^{Cre}*;Viaat*^{lxlx} mice suggesting that neonatal locomotion is not modulated by Renshaw cells. Furthermore, if Renshaw cells have an integral role in fictive locomotion, addition of mecamylamine, which depletes spiking activity of Renshaw cells (Nishimaru et al., 2006), should have limited impact on the locomotor rhythm in *Chrna2*^{Cre}*;Viaat*^{lxlx} cords. A comparable decrease in locomotor frequency was observed in both control and *Chrna2*^{Cre}*;Viaat*^{lxlx} mice, suggesting that the mecamylamine effect on fictive locomotion is likely due to the inhibition of nicotinic receptors on cells other than Renshaw cells.

When the NMDA concentration increased, the frequency of the locomotor rhythm increased due to a shortening of motor neuron bursting. Similar burst shortening was seen in *Chrna2*^{Cre}*;Viaat*^{lxlx} ventral roots, suggesting that Renshaw cells do not limit motor neuron bursting during fictive locomotion. Moreover, adult *Chrna2*^{Cre}*;Viaat*^{lxlx} mice behaved normally in all motor tasks, even when challenged, suggesting that Renshaw cells are not required for speed control, adaptation or motor coordination under these circumstances. We propose these results can be explained either by a redundancy in Renshaw cell function for fictive and physical locomotion,

JNeurosci Accepted Manuscript

or by compensatory mechanisms in the mutant mice.

Compensation in the Renshaw cell - motor neuron circuit

The absence of behavioral deficiencies in *Chrna2*^{Cre};*Viaat*^{lxlx} mice, suggest that the physiological role of Renshaw cells is potentially compensated for during network development. Network connectivity, function, synaptic strength and excitability are shaped by spontaneous activity in developing circuits throughout spinal cord maturation (Blankenship and Feller, 2010). Moreover, spontaneous activity in embryonic mice, mediated by cholinergic, glycinergic and GABAergic pathways, shapes the development and characteristics of spinal motor circuits (Hanson and Landmesser, 2003). Neural circuits have impressive capacities to generate 'normal' output activity even if circuit components, such as VIAAT-mediated neurotransmission, are removed (see review; Blankenship and Feller, 2010). Neurons maintain network activity levels within a defined physiological range by adjusting cellular excitability, rhythmogenic capabilities and the strength of excitatory and inhibitory synaptic inputs (De Zeeuw et al., 2003; Leao et al., 2004; Sapir et al., 2004; Harley et al., 2015). *In ovo* application of the $GABA_A$-receptor antagonist Gabazine, initially reduced spontaneous activity that later recovered with alterations to motor neuron excitability (Wilhelm and Wenner, 2008; Wilhelm et al., 2009). Further, a study of a mouse model of amyotrophic lateral sclerosis found that decreased GABA inhibition in the motor cortex was associated to hyperexcitable layer 5 pyramidal neurons and overall cortical excitability (Nieto-Gonzalez et al., 2011). These regulatory mechanisms could support the presumable compensatory changes in the recurrent inhibitory circuit found here; *Chrna2*^{Cre};*Viaat*^{lxlx} Renshaw cells became hyperexcitable whereas motor neurons have a lower input resistance, requiring a

JNeurosci Accepted Manuscript

larger current input to fire and therefore this may reflect the processes that operate to ensure a robust and stable motor output. This presumable compensation seemed surprisingly complementary; motor neurons and Renshaw cells had relatively comparable and opposite trends in changes to some neural properties that contribute to cellular excitability.

The observed alterations could partly be explained by the significant changes to motor neuron and Renshaw cell input resistance, however, changes to ion channel protein levels and the magnitude and contribution of ionic conductances also contribute to recovering inherent activity (Chub and O'Donovan, 1998; Desai et al., 1999; De Zeeuw et al., 2003; MacLean et al., 2003; Swensen and Bean, 2005; Leao et al., 2010; Wenner, 2014). Although identifying possible ionic changes within the recurrent inhibition circuit was outside the scope of this study, there were notable changes to the composition of the spontaneous inhibitory neurotransmitter release on *Chrna2*^{Cre}*;Viaat*^{lxlx} motor neurons (Fig. 6). This supports the further examination of ion channel contributions and possible modifications in future studies addressing compensation.

Compensatory adaptations in synaptic input

The modified cellular membrane properties within the *Chrna2*^{Cre}*;Viaat*^{lxlx} recurrent inhibitory circuit were coupled to a significant increase in the number of synaptic connections to motor neurons, which could be part of the compensation mechanism to balance the lower input resistance of motor neurons. *Chrna2*^{Cre}*;Viaat*^{lxlx} motor neurons had an increased number of presumable inhibitory calbindin^{+} contacts and excitatory VGLUT1 contacts. Interestingly, despite the increased number of VGLUT1 inputs, specific activation of these synapses by dorsal root stimulation generated a

JNeurosci Accepted Manuscript

motor neuron response of normal amplitude (monosynaptic stretch reflex). This observation lends support to a model where the hypoexcitable motor neurons develop more synapses (presumably stronger synaptic input) to generate normal motor output.

Since Renshaw cells are the predominant source of calbindin^{+} contacts in the ventral horn (Carr et al., 1998), we find it likely that the increased calbindin^{+} contacts on motor neurons arise from Renshaw cells. This phenomenon has been observed during disease progression in the *Sod1*^{G93A} mouse model, where Renshaw cell axonal sprouting gave rise to an increased number of calbindin^{+} Renshaw cell contacts on motor neurons (Wootz et al., 2013). The number of Renshaw cells appeared unaltered in *Chrna2*^{Cre}*;Viaat*^{lxlx} mice, suggesting that *Chrna2*^{Cre}*;Viaat*^{lxlx} Renshaw cells could have increased calbindin^{+} axonal connections to strengthen recurrent inhibition. In another mouse model of altered neuronal development, *engrailed*$^{-/-}$ mice, in which Renshaw cells and Ia inhibitory interneurons fail to develop, had a 50% reduction in the number of calbindin^{+} Renshaw cell- motor neuron contacts, whereas the total number of inhibitory synapses remained constant (Sapir et al., 2004). Locomotor behavior in *engrailed*$^{-/-}$ mice was unaffected, similar to *Chrna2*^{Cre}*;Viaat*^{lxlx} mice, illustrating how synaptic changes can be associated to compensation and maintenance of normal behavior.

Concluding remarks

In recent years, suggestions for the role of Renshaw cells have covered their involvement in speed and force regulation (Kiehn, 2006; Alvarez and Fyffe, 2007), through to sculpting the spiking activity of motor neurons (Pratt and Jordan, 1987; Brownstone and Bui, 2010). Our results support a role for Renshaw cells in modifying motor neuron activity, but in the absence of a locomotor phenotype, do not support a

JNeurosci Accepted Manuscript

812 direct role in speed or force regulation. However, we found a presumable
813 complementary compensation between motor neurons and Renshaw cells, which, in
814 spite of a role for Renshaw cells in locomotor circuits, could underlie the undisturbed
815 locomotor output in *Chrna2*^{Cre};*Viaat*^{lxlx} mice. In any case, our results highlight that
816 the spinal cord recurrent inhibitory circuit is endowed with several mechanisms to
817 maintain a purposeful output and indicate that further analysis of Renshaw cell
818 function should be addressed using acute silencing.
819
820
821

JNeurosci Accepted Manuscript

822 **References**
823

824 Alvarez, F.J., and Fyffe, R.E.W. (2007). The continuing case for the Renshaw cell. J.
825 Physiol. *584*, 31–45.

826 Andersson, L.S., Larhammar, M., Memic, F., Wootz, H., Schwochow, D., Rubin, C.-
827 J., Patra, K., Arnason, T., Wellbring, L., Hjälm, G., et al. (2012). Mutations in
828 DMRT3 affect locomotion in horses and spinal circuit function in mice. Nature *488*,
829 642–646.

830 Aubrey, K.R. (2016). Presynaptic control of inhibitory neurotransmitter content in
831 VIAAT containing synaptic vesicles. Neurochem. Int.

832 Betley, J.N., Wright, C.V.E., Kawaguchi, Y., Erdélyi, F., Szabó, G., Jessell, T.M., and
833 Kaltschmidt, J.A. (2009). Stringent specificity in the construction of a GABAergic
834 presynaptic inhibitory circuit. Cell *139*, 161–174.

835 Blankenship, A.G., and Feller, M.B. (2010). Mechanisms underlying spontaneous
836 patterned activity in developing neural circuits. Nat. Rev. Neurosci. *11*, 18–29.

837 Brownstone, R.M., and Bui, T.V. (2010). Spinal interneurons providing input to the
838 final common path during locomotion. Prog. Brain Res. *187*, 81–95.

839 Carr, P.A., Alvarez, F.J., Leman, E.A., and Fyffe, R.E. (1998). Calbindin D28k
840 expression in immunohistochemically identified Renshaw cells. Neuroreport *9*, 2657–
841 2661.

842 Chub, N., and O'Donovan, M.J. (1998). Blockade and recovery of spontaneous
843 rhythmic activity after application of neurotransmitter antagonists to spinal networks
844 of the chick embryo. J. Neurosci. Off. J. Soc. Neurosci. *18*, 294–306.

845 Desai, N.S., Rutherford, L.C., and Turrigiano, G.G. (1999). Plasticity in the intrinsic
846 excitability of cortical pyramidal neurons. Nat. Neurosci. *2*, 515–520.

847 Eccles, J.C., Fatt, P., and Koketsu, K. (1954). Cholinergic and inhibitory synapses in a
848 pathway from motor-axon collaterals to motoneurones. J. Physiol. *126*, 524–562.

849 Enjin, A., Rabe, N., Nakanishi, S.T., Vallstedt, A., Gezelius, H., Memic, F., Lind, M.,
850 Hjalt, T., Tourtellotte, W.G., Bruder, C., et al. (2010). Identification of novel spinal
851 cholinergic genetic subtypes disclose Chodl and Pitx2 as markers for fast motor
852 neurons and partition cells. J. Comp. Neurol. *518*, 2284–2304.

853 Fujiyama, F., Furuta, T., and Kaneko, T. (2001). Immunocytochemical localization of
854 candidates for vesicular glutamate transporters in the rat cerebral cortex. J. Comp.
855 Neurol. *435*, 379–387.

856 Geiman, E.J., Knox, M.C., and Alvarez, F.J. (2000). Postnatal maturation of
857 gephyrin/glycine receptor clusters on developing Renshaw cells. J. Comp. Neurol.
858 *426*, 130–142.

859 Gosgnach, S., Lanuza, G.M., Butt, S.J.B., Saueressig, H., Zhang, Y., Velasquez, T.,

JNeurosci Accepted Manuscript

860 Riethmacher, D., Callaway, E.M., Kiehn, O., and Goulding, M. (2006). V1 spinal
861 neurons regulate the speed of vertebrate locomotor outputs. Nature *440*, 215–219.

862 Goulding, M. (2009). Circuits controlling vertebrate locomotion: moving in a new
863 direction. Nat. Rev. Neurosci. *10*, 507–518.

864 Hanson, M.G., and Landmesser, L.T. (2003). Characterization of the circuits that
865 generate spontaneous episodes of activity in the early embryonic mouse spinal cord. J.
866 Neurosci. Off. J. Soc. Neurosci. *23*, 587–600.

867 Harley, C.M., Reilly, M.G., Stewart, C., Schlegel, C., Morley, E., Puhl, J.G., Nagel,
868 C., Crisp, K.M., and Mesce, K.A. (2015). Compensatory plasticity restores
869 locomotion after chronic removal of descending projections. J. Neurophysiol. *113*,
870 3610–3622.

871 Kanning, K.C., Kaplan, A., and Henderson, C.E. (2010). Motor neuron diversity in
872 development and disease. Annu. Rev. Neurosci. *33*, 409–440.

873 Kiehn, O. (2006). Locomotor circuits in the mammalian spinal cord. Annu. Rev.
874 Neurosci. *29*, 279–306.

875 Kullander, K. (2005). Genetics moving to neuronal networks. Trends Neurosci. *28*,
876 239–247.

877 Leao, K.E., Leao, R.N., Deardorff, A.S., Garrett, A., Fyffe, R., and Walmsley, B.
878 (2010). Sound stimulation modulates high-threshold K(+) currents in mouse auditory
879 brainstem neurons. Eur. J. Neurosci. *32*, 1658–1667.

880 Leao, R.N., Oleskevich, S., Sun, H., Bautista, M., Fyffe, R.E.W., and Walmsley, B.
881 (2004). Differences in Glycinergic mIPSCs in the Auditory Brain Stem of Normal and
882 Congenitally Deaf Neonatal Mice. J. Neurophysiol. *91*, 1006–1012.

883 Leao, R.N., Mikulovic, S., Leao, K.E., Munguba, H., Gezelius, H., Enjin, A., Patra,
884 K., Eriksson, A., Loew, L.M., Tort, A.B.L., et al. (2012). OLM interneurons
885 differentially modulate CA3 and entorhinal inputs to hippocampal CA1 neurons. Nat.
886 Neurosci. *15*, 1524–1530.

887 Li, Y., and Burke, R.E. (2001). Short-term synaptic depression in the neonatal mouse
888 spinal cord: effects of calcium and temperature. J. Neurophysiol. *85*, 2047–2062.

889 MacLean, J.N., Zhang, Y., Johnson, B.R., and Harris-Warrick, R.M. (2003). Activity-
890 Independent Homeostasis in Rhythmically Active Neurons. Neuron *37*, 109–120.

891 Madisen, L., Zwingman, T.A., Sunkin, S.M., Oh, S.W., Zariwala, H.A., Gu, H., Ng,
892 L.L., Palmiter, R.D., Hawrylycz, M.J., Jones, A.R., et al. (2010). A robust and high-
893 throughput Cre reporting and characterization system for the whole mouse brain. Nat.
894 Neurosci. *13*, 133–140.

895 McCrea, D.A., Pratt, C.A., and Jordan, L.M. (1980). Renshaw cell activity and
896 recurrent effects on motoneurons during fictive locomotion. J. Neurophysiol. *44*, 475–
897 488.

JNeurosci Accepted Manuscript

898 Mentis, G.Z., Alvarez, F.J., Bonnot, A., Richards, D.S., Gonzalez-Forero, D., Zerda,
899 R., and O'Donovan, M.J. (2005). Noncholinergic excitatory actions of motoneurons
900 in the neonatal mammalian spinal cord. Proc. Natl. Acad. Sci. U. S. A. *102*, 7344–
901 7349.

902 Mentis, G.Z., Siembab, V.C., Zerda, R., O'Donovan, M.J., and Alvarez, F.J. (2006).
903 Primary Afferent Synapses on Developing and Adult Renshaw Cells. J. Neurosci. *26*,
904 13297–13310.

905 Metz, G.A., and Whishaw, I.Q. (2009). The ladder rung walking task: a scoring
906 system and its practical application. J. Vis. Exp. JoVE.

907 Mor, Y., and Lev-Tov, A. (2007). Analysis of rhythmic patterns produced by spinal
908 neural networks. J. Neurophysiol. *98*, 2807–2817.

909 Myers, C.P., Lewcock, J.W., Hanson, M.G., Gosgnach, S., Aimone, J.B., Gage, F.H.,
910 Lee, K.-F., Landmesser, L.T., and Pfaff, S.L. (2005). Cholinergic input is required
911 during embryonic development to mediate proper assembly of spinal locomotor
912 circuits. Neuron *46*, 37–49.

913 Nakanishi, S.T., and Whelan, P.J. (2010). Diversification of intrinsic motoneuron
914 electrical properties during normal development and botulinum toxin-induced muscle
915 paralysis in early postnatal mice. J. Neurophysiol. *103*, 2833–2845.

916 Nieto-Gonzalez, J.L., Moser, J., Lauritzen, M., Schmitt-John, T., and Jensen, K.
917 (2011). Reduced GABAergic inhibition explains cortical hyperexcitability in the
918 wobbler mouse model of ALS. Cereb. Cortex N. Y. N 1991 *21*, 625–635.

919 Nishimaru, H., Restrepo, C.E., and Kiehn, O. (2006). Activity of Renshaw cells
920 during locomotor-like rhythmic activity in the isolated spinal cord of neonatal mice. J.
921 Neurosci. Off. J. Soc. Neurosci. *26*, 5320–5328.

922 Noga, B.R., Shefchyk, S.J., Jamal, J., and Jordan, L.M. (1987). The role of Renshaw
923 cells in locomotion: antagonism of their excitation from motor axon collaterals with
924 intravenous mecamylamine. Exp. Brain Res. *66*, 99–105.

925 Perry, S., Gezelius, H., Larhammar, M., Hilscher, M.M., Lamotte d'Incamps, B.,
926 Leao, K.E., and Kullander, K. (2015). Firing properties of Renshaw cells defined by
927 Chrna2 are modulated by hyperpolarizing and small conductance ion currents Ih and
928 ISK. Eur. J. Neurosci. n/a – n/a.

929 Pratt, C.A., and Jordan, L.M. (1987). Ia inhibitory interneurons and Renshaw cells as
930 contributors to the spinal mechanisms of fictive locomotion. J. Neurophysiol. *57*, 56–
931 71.

932 Rabe, N., Gezelius, H., Vallstedt, A., Memic, F., and Kullander, K. (2009). Netrin-1-
933 dependent spinal interneuron subtypes are required for the formation of left-right
934 alternating locomotor circuitry. J. Neurosci. Off. J. Soc. Neurosci. *29*, 15642–15649.

935 Rahman, J., Besser, S., Schnell, C., Eulenburg, V., Hirrlinger, J., Wojcik, S.M., and
936 Hülsmann, S. (2015). Genetic ablation of VIAAT in glycinergic neurons causes a
937 severe respiratory phenotype and perinatal death. Brain Struct. Funct. *220*, 2835–

JNeurosci Accepted Manuscript

938 2849.

939 RENSHAW, B. (1946). Observations on interaction of nerve impulses in the gray
940 matter and on the nature of central inhibition. Am. J. Physiol. *146*, 443–448.

941 Sapir, T., Geiman, E.J., Wang, Z., Velasquez, T., Mitsui, S., Yoshihara, Y., Frank, E.,
942 Alvarez, F.J., and Goulding, M. (2004). Pax6 and engrailed 1 regulate two distinct
943 aspects of renshaw cell development. J. Neurosci. Off. J. Soc. Neurosci. *24*, 1255–
944 1264.

945 Swensen, A.M., and Bean, B.P. (2005). Robustness of burst firing in dissociated
946 purkinje neurons with acute or long-term reductions in sodium conductance. J.
947 Neurosci. Off. J. Soc. Neurosci. *25*, 3509–3520.

948 Tong, Q., Ye, C.-P., Jones, J.E., Elmquist, J.K., and Lowell, B.B. (2008). Synaptic
949 release of GABA by AgRP neurons is required for normal regulation of energy
950 balance. Nat. Neurosci. *11*, 998–1000.

951 Wegmeyer, H., Egea, J., Rabe, N., Gezelius, H., Filosa, A., Enjin, A., Varoqueaux, F.,
952 Deininger, K., Schnütgen, F., Brose, N., et al. (2007). EphA4-dependent axon
953 guidance is mediated by the RacGAP alpha2-chimaerin. Neuron *55*, 756–767.

954 Wenner, P. (2014). Homeostatic synaptic plasticity in developing spinal networks
955 driven by excitatory GABAergic currents. Neuropharmacology *78*, 55–62.

956 Wilhelm, J.C., and Wenner, P. (2008). GABAA transmission is a critical step in the
957 process of triggering homeostatic increases in quantal amplitude. Proc. Natl. Acad.
958 Sci. U. S. A. *105*, 11412–11417.

959 Wilhelm, J.C., Rich, M.M., and Wenner, P. (2009). Compensatory changes in cellular
960 excitability, not synaptic scaling, contribute to homeostatic recovery of embryonic
961 network activity. Proc. Natl. Acad. Sci. U. S. A. *106*, 6760–6765.

962 Windhorst, U. (1996). On the role of recurrent inhibitory feedback in motor control.
963 Prog. Neurobiol. *49*, 517–587.

964 Wojcik, S.M., Katsurabayashi, S., Guillemin, I., Friauf, E., Rosenmund, C., Brose, N.,
965 and Rhee, J.-S. (2006). A shared vesicular carrier allows synaptic corelease of GABA
966 and glycine. Neuron *50*, 575–587.

967 Wootz, H., Fitzsimons-Kantamneni, E., Larhammar, M., Rotterman, T.M., Enjin, A.,
968 Patra, K., André, E., Van Zundert, B., Kullander, K., and Alvarez, F.J. (2013).
969 Alterations in the motor neuron-renshaw cell circuit in the Sod1(G93A) mouse model.
970 J. Comp. Neurol. *521*, 1449–1469.

971 Zagoraiou, L., Akay, T., Martin, J.F., Brownstone, R.M., Jessell, T.M., and Miles,
972 G.B. (2009). A cluster of cholinergic premotor interneurons modulates mouse
973 locomotor activity. Neuron *64*, 645–662.

974 De Zeeuw, C.I., Chorev, E., Devor, A., Manor, Y., Van Der Giessen, R.S., De Jeu,
975 M.T., Hoogenraad, C.C., Bijman, J., Ruigrok, T.J.H., French, P., et al. (2003).
976 Deformation of network connectivity in the inferior olive of connexin 36-deficient

JNeurosci Accepted Manuscript

977 mice is compensated by morphological and electrophysiological changes at the single
978 neuron level. J. Neurosci. Off. J. Soc. Neurosci. *23*, 4700–4711.

979 Zhang, Y., Narayan, S., Geiman, E., Lanuza, G.M., Velasquez, T., Shanks, B., Akay,
980 T., Dyck, J., Pearson, K., Gosgnach, S., et al. (2008). V3 Spinal Neurons Establish a
981 Robust and Balanced Locomotor Rhythm during Walking. Neuron *60*, 84–96.

982
983
984

JNeurosci Accepted Manuscript

Figure Legends

Figure 1. *Chrna2*^{Cre} labels Renshaw cell-derived synapses on motor neurons

(***A***) Schematic illustration of the Recurrent inhibitory (Renshaw cell (RC) - Motor neuron (MN)) circuit. Calbindin and *Chrna2*$^{+}$ Renshaw cells (red) form inhibitory VIAAT synapses on motor neurons and are reciprocally innervated by cholinergic motor neuron axons (blue). (***B***) Immunohistochemistry of calbindin^{+} (left) and VIAAT^{+} (right) contacts derived from *Chrna2*^{Cre}*; R26.lsl.tdTomato*$^{+}$ cells on motor neurons (ChAT) in the lumbar spinal cord of adult mice. Inset shows overlap between VIAAT, calbindin and *Chrna2*^{Cre}*; R26.lsl.tdTomato.* (***C***) A schematic illustration of a hemisected spinal cord slice detailing the antidromic ventral root setup (left) with example traces showing the response of a *Chrna2*^{Cre}*; R26.lsl.tdTomato*$^{+}$ cell to ventral root stimulation in the absence (red) and presence (black) of mecamylamine (right).

Figure 2. *Chrna2*^{Cre}*;Viaat*^{lxlx} motor neurons develop with altered synaptic inputs

(***A***) *In situ* hybridization for *Viaat* (red) combined with an immunohistochemistry for calbindin (green) confirmed that Renshaw cells in the lumbar spinal cord did not express *Viaat* mRNA in adult *Chrna2*^{Cre}*;Viaat*^{lxlx} mice (right). All control (*Viaat*$^{lx/lx}$) calbindin^{+} Renshaw cells expressed *Viaat mRNA* (left). (***B***) Immunohistochemistry of calbindin^{+} Renshaw cells (green) and motor axon collaterals stained by VAChT or ChAT (red), co-localized with synaptophysin (blue, upper panel). Inset and arrows show triple overlap (upper panels) or VAChT^{+} and calbindin^{+} signals in close opposition (lower panels). Motor neuron innervation of Renshaw cells was unchanged in *Chrna2*^{Cre}*;Viaat*^{lxlx} mice. (***C***) Immunohistochemistry of calbindin^{+} Renshaw cell synapses (green, arrows) and ChAT^{+} C-boutons (red) on motor neurons, co-localized with synaptophysin (blue). Inset shows triple overlap. *Chrna2*^{Cre}*;Viaat*^{lxlx} motor

JNeurosci Accepted Manuscript

neurons had an increased number of calbindin synapses. (***D***) Immunohistochemistry of VGLUT1^{+} contacts (green), co-localized with synaptophysin^{+} (blue), on ChAT^{+} motor neuron soma and proximal dendrites (red). Inset and arrows show triple overlap. The number of VGLUT1^{+} synapses was increased in *Chrna2*^{Cre}*;Viaat*^{lxlx} motor neurons. Data represents mean ± SEMs. Mann-Whitney U-test, * $p < 0.05$, *** $p < 0.001$.

Figure 3. *Chrna2*^{Cre}*;Viaat*^{lxlx} mice had normal stretch reflex parameters and motor behavior despite an increased number of proprioceptive synapses

(***A***) Schematic of the spinal cord illustrating the stretch reflex experimental setup and examples of the averaged ventral root responses to dorsal root stimulation in control *Viaat*$^{lx/lx}$ (left) and *Chrna2*^{Cre}*;Viaat*^{lxlx} (right) mice. Horizontal arrows indicate monosynaptic and polysynaptic peaks, vertical arrows indicate onset of monosynaptic and polysynaptic episodes. (***B, C***) The amplitudes **(B)** and latencies **(C)** of the mono- and polysynaptic peaks were not altered in neonatal *Chrna2*^{Cre}*;Viaat*^{lxlx} mice. (***D***) Synaptic depression of the monosynaptic amplitude in response to 1 Hz (left) and 8 Hz (right) stimulus volley was not altered in *Chrna2*^{Cre}*;Viaat*^{lxlx} mice. (***E-H***) *Chrna2*^{Cre}*;Viaat*^{lxlx} mice exhibit normal motor behavior across a range of tasks. (***E***) Fore paw grip strength was similar between adult control and *Chrna2*^{Cre}*;Viaa*^{lxlx} mice. (***F***) Time to fall on the steady speed rotarod at 5, 10, 15 and 20 rpm was unaffected in *Chrna2*^{Cre}*;Viaat*^{lxlx} mice compared to controls. (***G***) *Chrna2*^{Cre}*;Viaat*^{lxlx} mice maintained the rotational speed of the accelerating rotarod and fell at a similar speed compared to control mice. (***H***) The average number of hind foot slips (left) and time to cross (right) a wooden beam was similar between *Chrna2*^{Cre}*;Viaat*^{lxlx} and control mice. Data represent mean ± SEMs; two-tailed student's T-test.

JNeurosci Accepted Manuscript

Figure 4. *Chrna2^{Cre};Viaat^{lxlx}* mice exhibit normal locomotor-like activity

(*A*) Schematic drawing of an isolated spinal cord with recording electrodes placed on the left (l) and right (r) lumbar (L) 2 and L5 ventral roots. Raw traces of locomotor-like activity from ventral root recordings from control (*Viaat$^{lx/lx}$*) and *Chrna2^{Cre};Viaat^{lxlx}* cords during fictive locomotion. The rectified, smoothened trace (blue) defined the burst, interburst and cycle periods. **(*B*)** Coherence power spectra of left/right (l/r) alternation activity recorded from lL2 vs. rL2 ventral roots and flexor/extensor (f/e) alternation from L2 vs. L5 ventral roots from control and *Chrna2^{Cre};Viaat^{lxlx}* spinal cords. The coherence power was normalized to a color-graded scale (right). White boxed region denotes the area used for coherence and frequency analysis; black line delineates the cone of influence; scale bar 40 s. **(*C*)** Circular statistic analysis confirmed an unchanged locomotor pattern in *Chrna2^{Cre};Viaat^{lxlx}* cords; control and *Chrna2^{Cre};Viaat^{lxlx}* mice displayed normal left/right and flexor/extensor alternation. Arrows denote the mean phase value given by the coherence band where a value near 0° represents synchrony and a value near 180° represents alternation; dashed inner line denotes significance (0.8, Rayleigh test). **(*D, E*)** The mean locomotor frequency (***D***) and coherence (***E***) for both left/right and flexion/extension coordination was unchanged between control and *Chrna2^{Cre};Viaat^{lxlx}* cords. **(*F*)** The mean cycle period, burst duration and interburst duration was normal in *Chrna2^{Cre};Viaat^{lxlx}* mice. **(*G*)** The coefficient of variation (CoV) for each burst parameter; cycle period, burst duration and interburst duration were normal in *Chrna2^{Cre};Viaat^{lxlx}* mice. Data represents mean ± SEMs; two-tailed Student's T-test.

JNeurosci Accepted Manuscript

Figure 5. Mecamylamine and NMDA had similar effects on the fictive locomotor rhythm

(***A***) Example raw traces of locomotor-like activity recorded from ventral roots of control (*Viaat*^{lxlx}) and *Chrna2*^{Cre}*;Viaat*^{lxlx} spinal cords after application of mecamylamine (50 μM) to the perfusate. The rectified, smoothened trace is shown in blue. (***B***) Coherence power spectra of left/right (l/r) alternation activity after exposure to mecamylamine for 50 minutes. Scale bar 40 s. (***C***) Application of mecamylamine did not alter the locomotor pattern in control or *Chrna2*^{Cre}*;Viaat*^{lxlx} cords; normal left/right and flexor/extensor alternation was maintained. Arrows denote the mean phase value given by the coherence band; dashed inner line denotes significance. (***D***) Mecamylamine induced a similar reduction in the frequency (left) and coherence (right) in *Chrna2*^{Cre}*;Viaat*^{lxlx} and control spinal cords. (***E***) Mecamylamine (Mec) increased the cycle period, burst and interburst duration as well as the coefficient of variation (CoV, right) for these parameters during locomotor-like activity in both control and *Chrna2*^{Cre}*;Viaat*^{lxlx} cords compared to baseline (Base). (***F***) Increasing NMDA concentrations increased the locomotor frequency and coherence in both control and *Chrna2*^{Cre}*;Viaat*^{lxlx} cords. (***G-I***) Increasing NMDA concentrations shortened the locomotor cycle period (***G***), burst (***H***) and interburst (***I***) duration but did not influence the coefficient of variation for these parameters during locomotor-like activity in both control and *Chrna2*^{Cre}*;Viaat*^{lxlx} cords. Data represents mean ± SEMs; two-tailed Student's T-test; two-way ANOVA.

Figure 6. Neonatal lumbar motor neurons receive lower frequency inhibitory spontaneous release in *Chrna2*^{Cre}*;Viaat*^{lxlx} mice

(A) Schematic drawing depicting the lost Renshaw cell (RC) VIAAT mediated

JNeurosci Accepted Manuscript

inhibition onto motor neurons (MN, motor neurons; IaIN, Ia inhibitory interneurons) in *Chrna2*^{Cre};*Viaat*^{lxlx} mice ***(B)*** Example traces of lumbar motor neuron mIPSCs before (left) and following PTX application (right) for control (*Viaat*^{lxlx}, top) and *Chrna2*^{Cre};*Viaat*^{lxlx} (bottom) mice. ***(C)*** Box plot of mIPSC frequencies for control (n = 8), control +PTX (n = 7), *Chrna2*^{Cre};*Viaat*^{lxlx} (n = 7) and *Chrna2*^{Cre};*Viaat*^{lxlx} +PTX (n = 7). ***(D)*** Example mIPSCs (50 overlaps in grey and mean in black) are shown before (left) and during PTX application (right) for control (top) and *Chrna2*^{Cre};*Viaat*^{lxlx} (bottom) mice. ***(E)*** Box plot of mIPSC amplitudes. ***(F)*** Box plot of mIPSC rise times. Data represents mean ± SEM, two-tailed Student's T-test; * $p < 0.05$, ** $p < 0.01$, *** $p < 0.001$.

Figure 7. VIAAT-mediated Renshaw cell signaling is required for development of motor neuron and Renshaw cell electrical properties

(***A***) Example action potential traces from control (black) and *Chrna2*^{Cre};*Viaat*^{lxlx} (grey) motor neurons (left) and Renshaw cells (right). Arrows indicate the action potential (AP) threshold, dashed grey lines highlight the AHP rise and half-width for the Renshaw cells, while motor neurons required a suprathreshold current injection to compare AHP between genotypes (see inset on right). (***B***) Control (black) and *Chrna2*^{Cre};*Viaat*^{lxlx} (grey) motor neurons have a similar spike frequency in response to depolarizing injected current. Inset; average spike frequency (F) for control and *Chrna2*^{Cre};*Viaat*^{lxlx} per injected current block; A: 0 - 800 pA, B: 0 – 1250 pA, C: 850 – 1900 pA, D: 1300 – 3500 pA. (***C***) *Chrna2*^{Cre};*Viaat*^{lxlx} Renshaw cells (grey) had a slower firing frequency than control Renshaw cells (black) in response to increasing depolarizing current steps. (***D***) The percentage change, either increase or decrease, in action potential properties from both *Chrna2*^{Cre};*Viaat*^{lxlx} motor neurons (dark grey)

JNeurosci Accepted Manuscript

and *Chrna2*^{Cre}*;Viaat*^{lxlx} Renshaw cells (light grey) compared to control animals. Data represents mean ± SEMs; two-tailed Student's T-test, Mann-Whitney U-Test; * $p < 0.05$, ** $p < 0.01$, *** $p < 0.001$.

Table 1. Locomotor behaviour is unaffected in *Chrna2*^{Cre}*;Viaat*$^{lx/lx}$ mice. Data represents mean ± SEM. Control n = 9; *Chrna2*^{Cre}*;Viaat*$^{lx/lx}$ n = 8.

Table 2. Electrical properties of the Recurrent inhibition circuit are altered in *Chrna2*^{Cre}*;Viaat*$^{lx/lx}$ mice. Data represents mean ± SEM. Motor neurons, control n = 13; *Chrna2*^{Cre}*;Viaat*$^{lx/lx}$ n = 9. Renshaw cells, control n = 13; *Chrna2*^{Cre}*;Viaat*$^{lx/lx}$ n = 13. * $p < 0.05$, ** $p < 0.01$, *** $p < 0.001$.

JNeurosci Accepted Manuscript

Figure. 1.

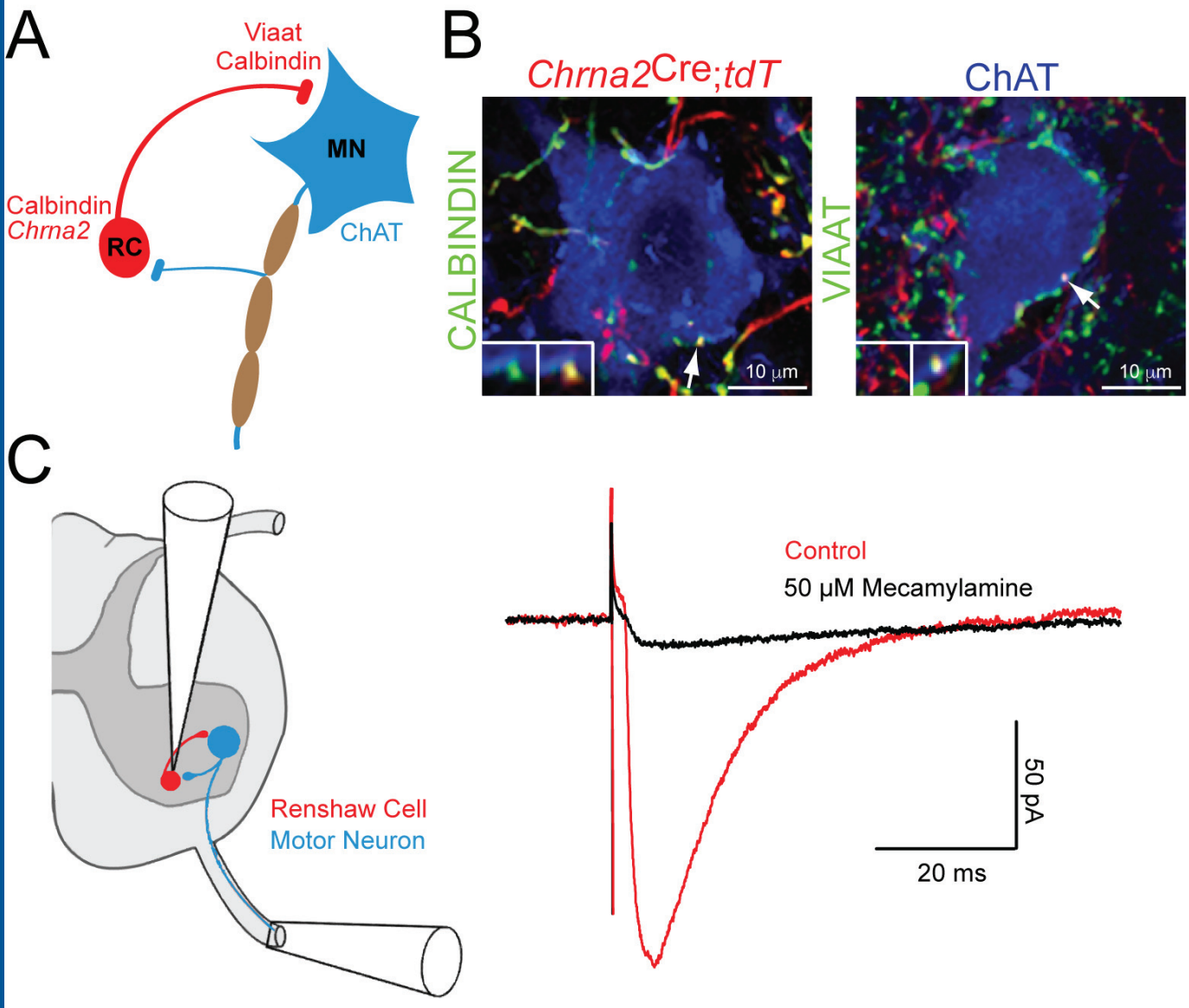

JNeurosci Accepted Manuscript

Figure. 2.

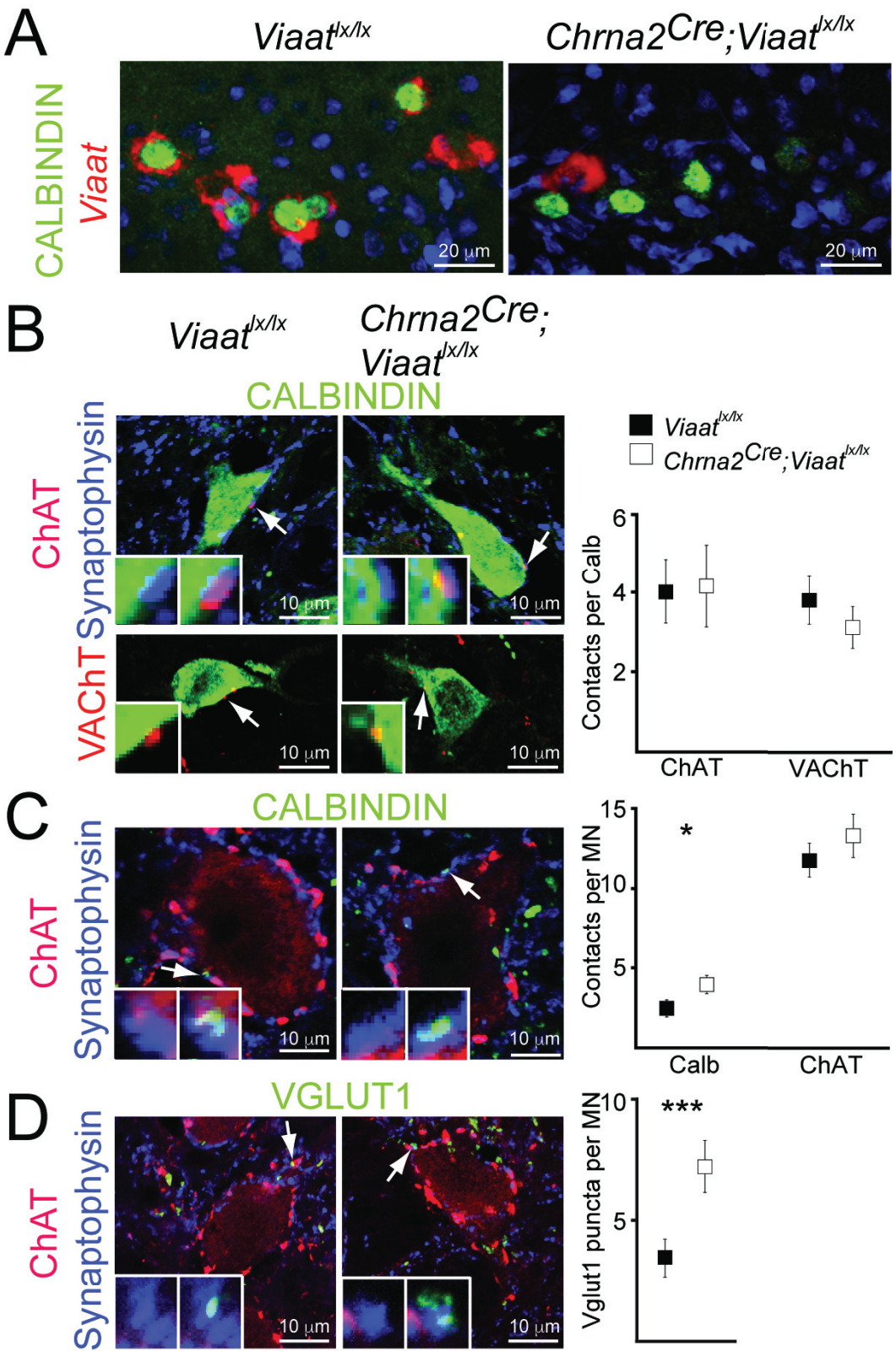

JNeurosci Accepted Manuscript

Figure 3.

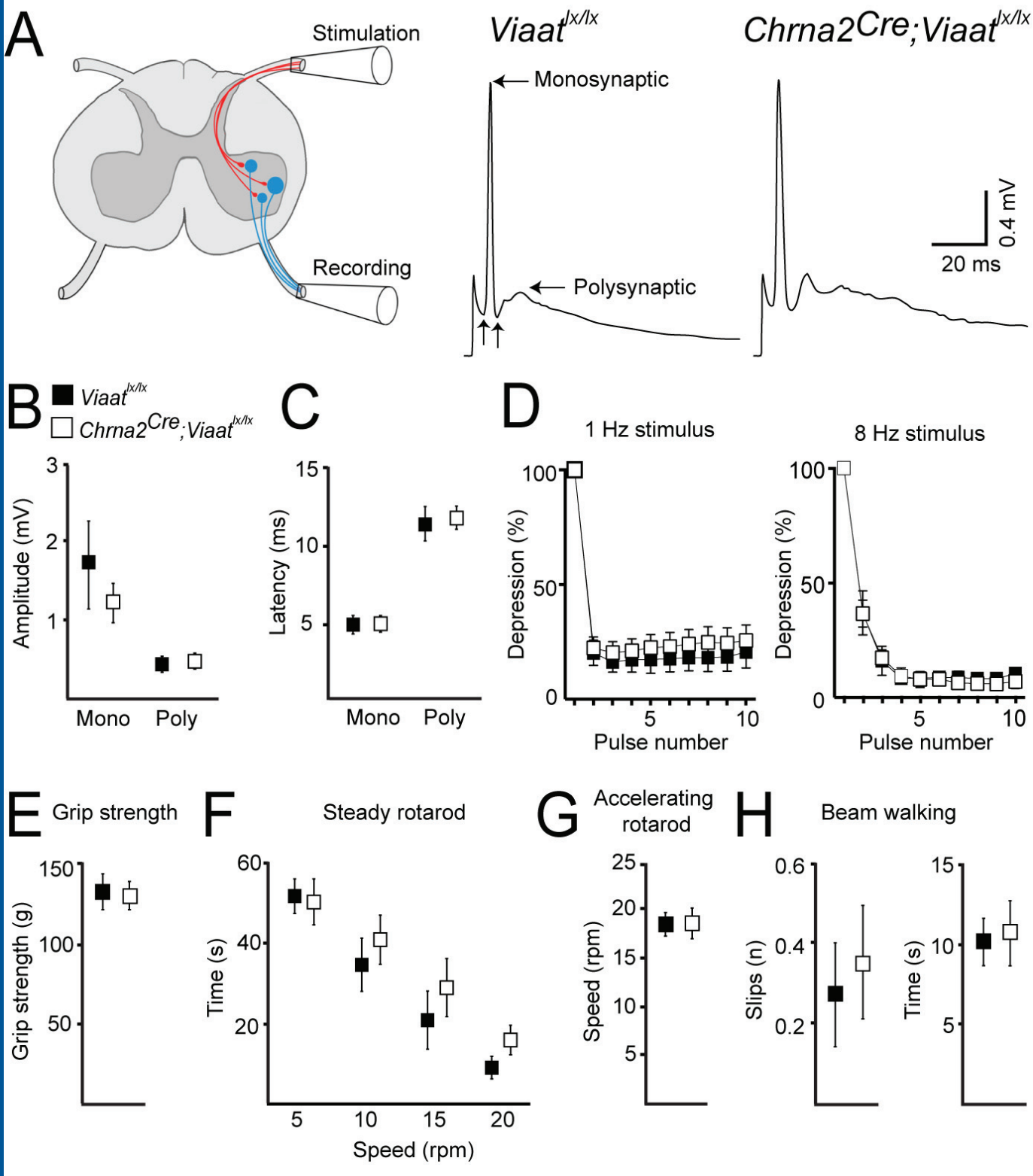

JNeurosci Accepted Manuscript

Figure 4.

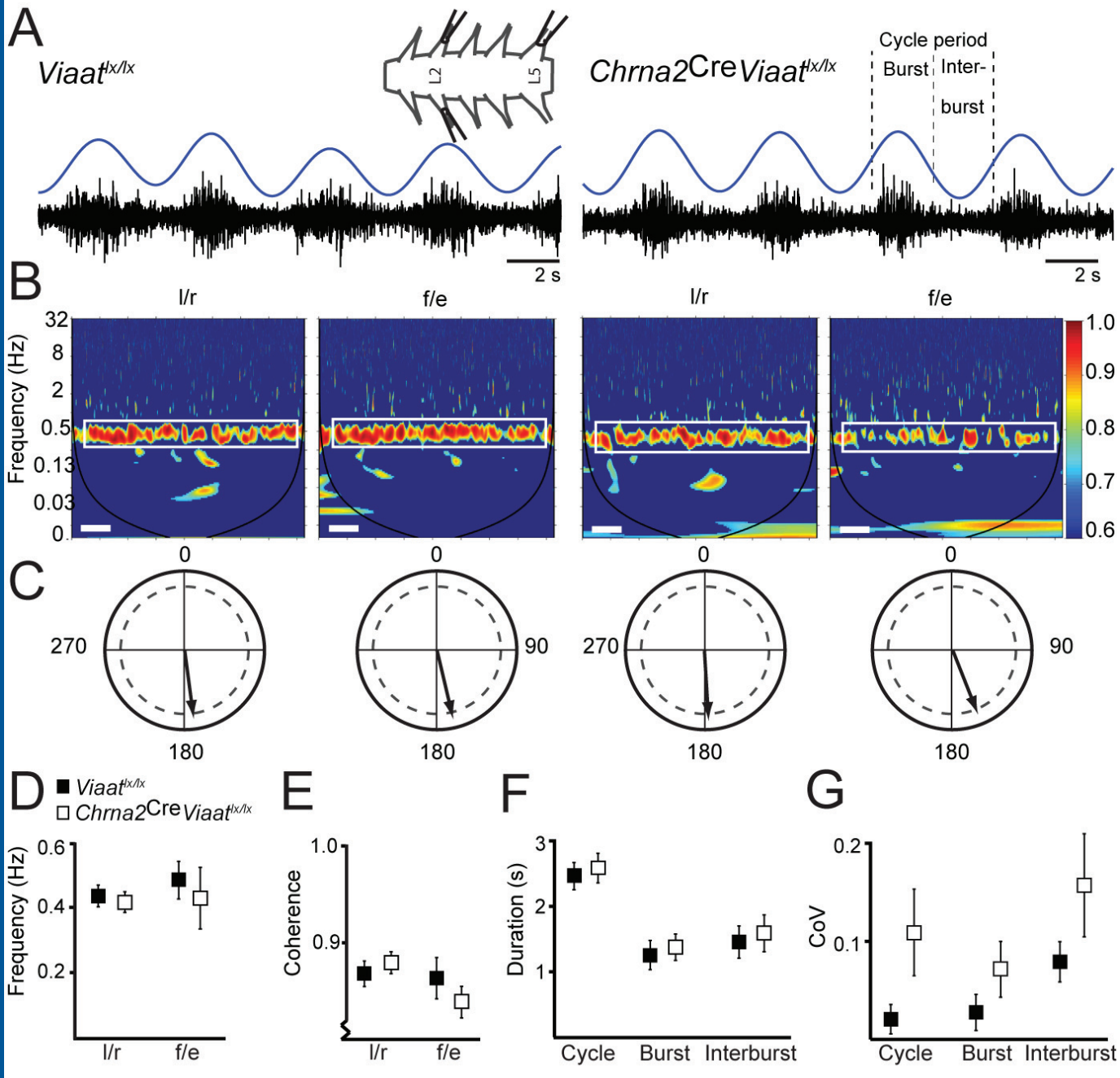

JNeurosci Accepted Manuscript

Figure 5.

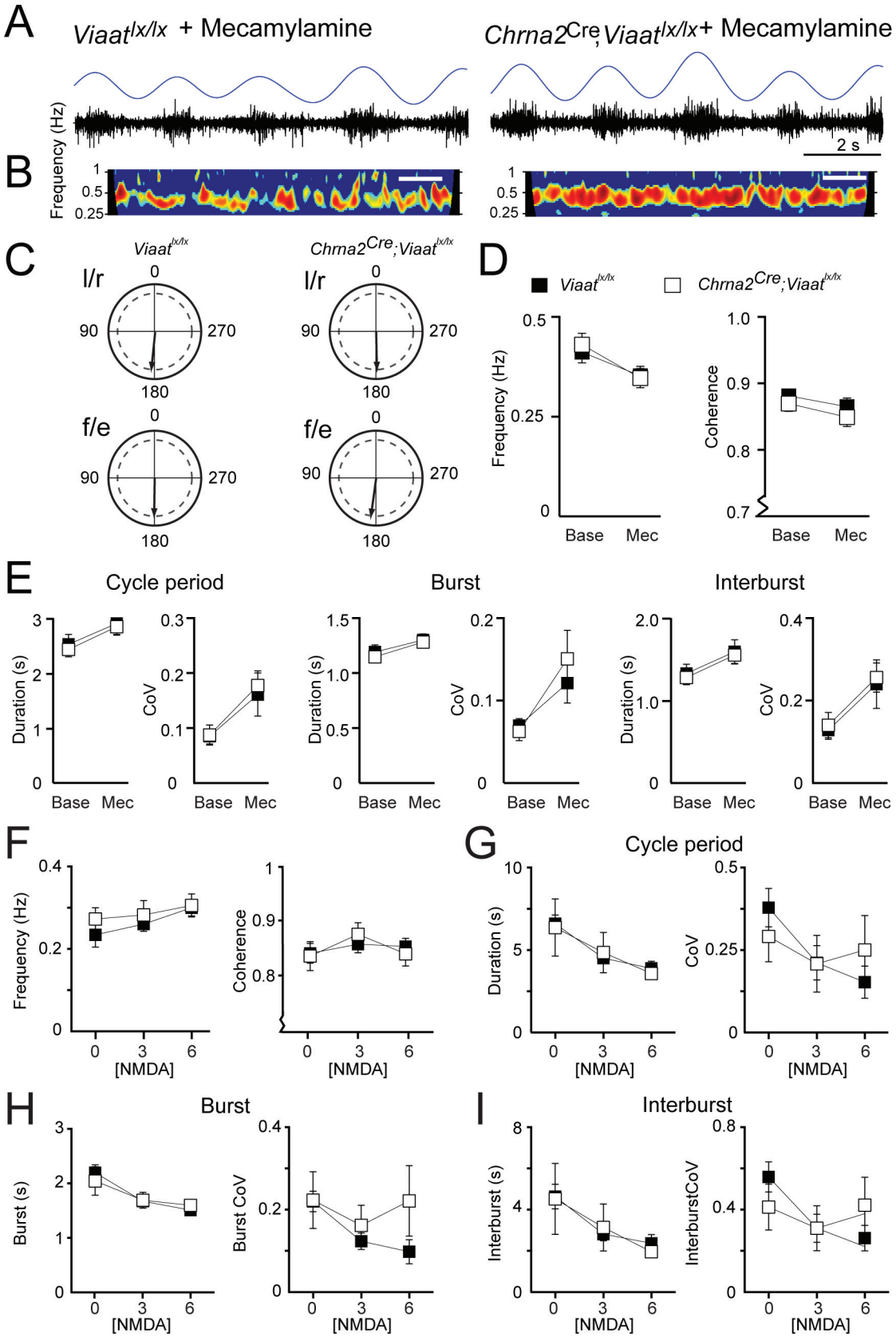

JNeurosci Accepted Manuscript

Figure 6.

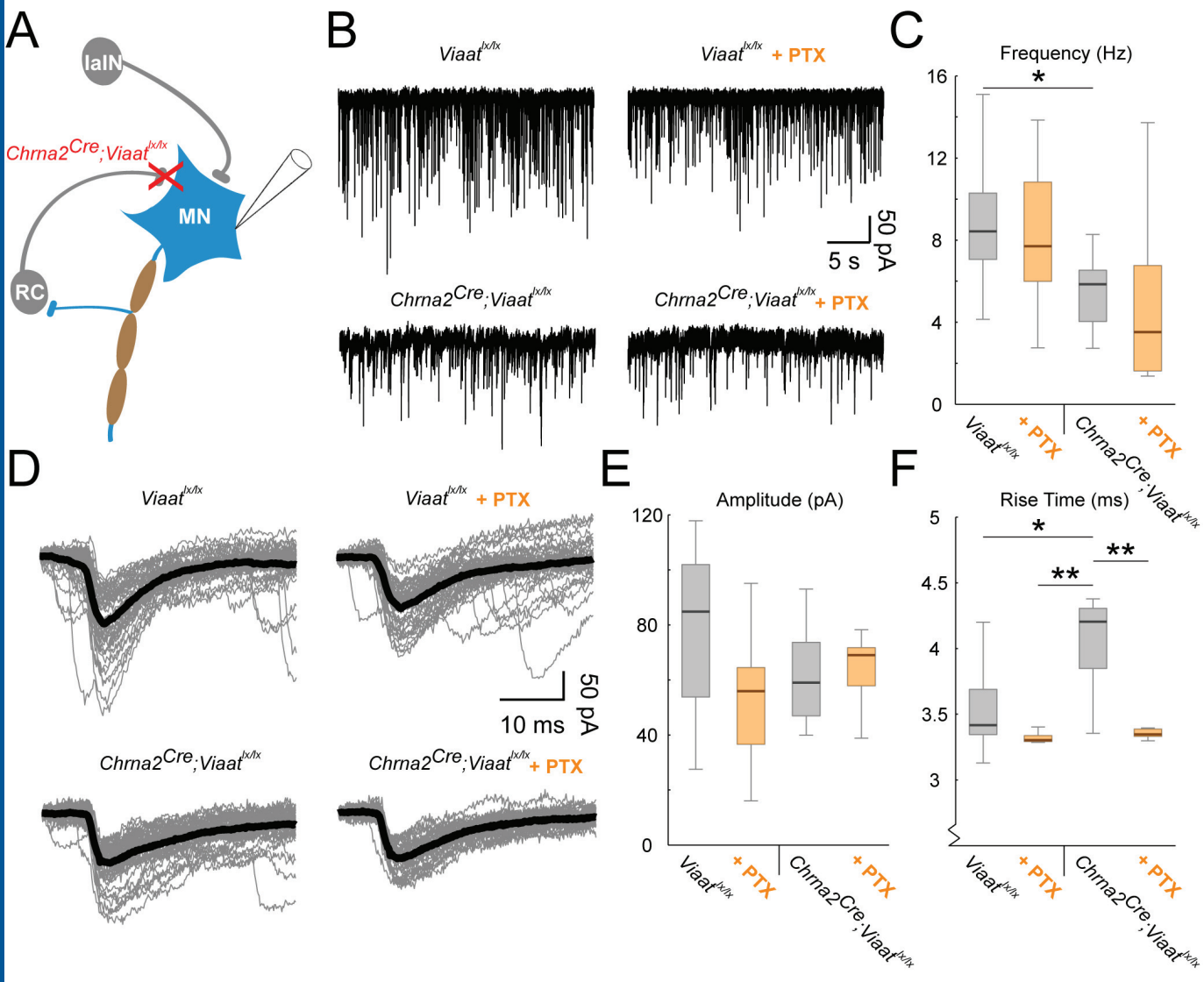

JNeurosci Accepted Manuscript

Figure 7.

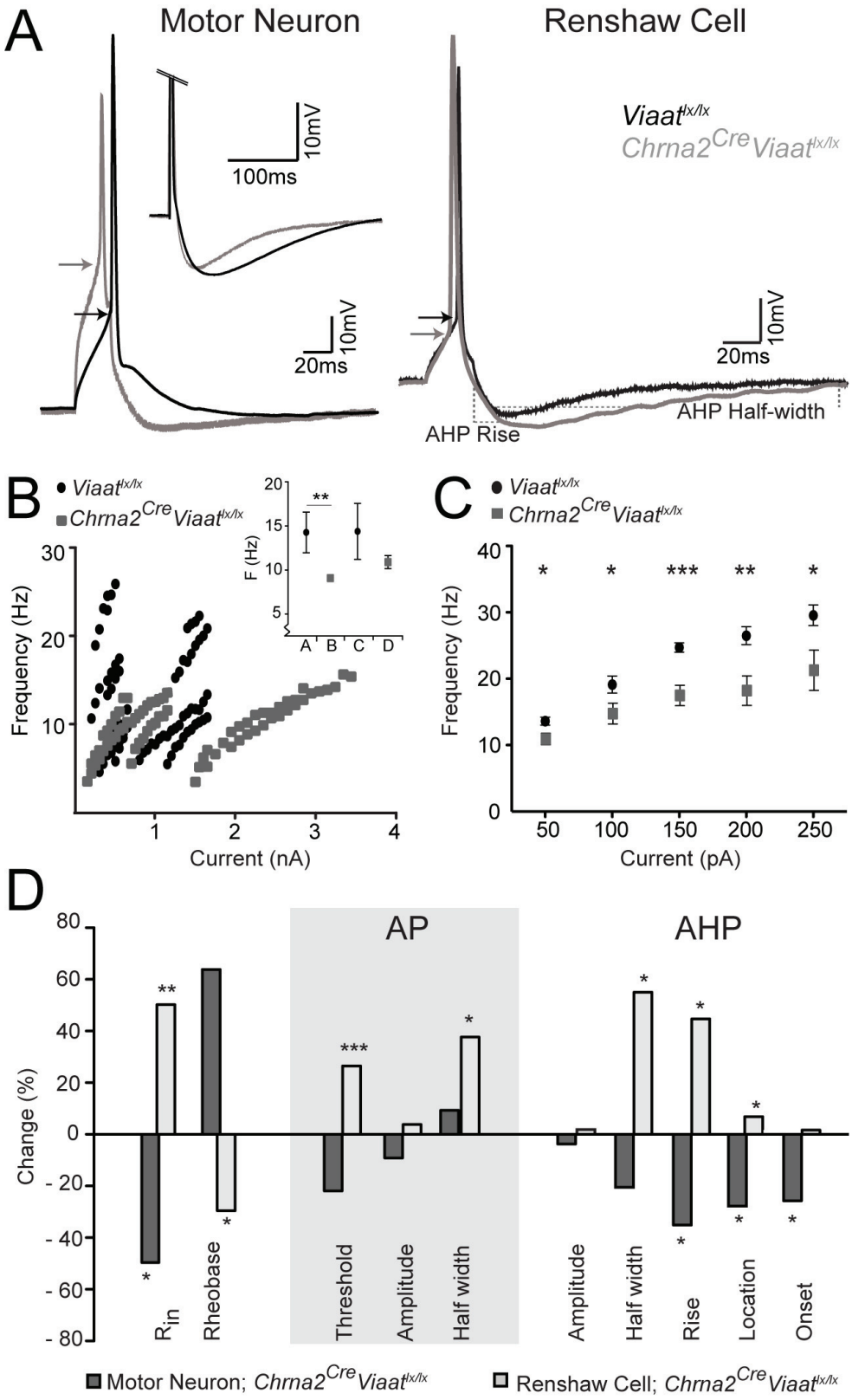

JNeurosci Accepted Manuscript

Removal of *Viaat* from the recurrent inhibitory circuit does not affect adult locomotor behaviour.

	Forelimbs			Hindlimbs		
	Control	*Chrna2*^{Cre};*Viaat*$^{lx/lx}$	P-Value	Control	*Chrna2*^{Cre};*Viaat*$^{lx/lx}$	P-Value
Stride time (ms)	264.8 ± 5.9	252.5 ± 5.8	0.18	266.0 ± 5.4	269.0 ± 8.2	0.77
Stance time (ms)	149.7 ± 7.6	140.9 ± 9.2	0.47	153.9 ± 5.3	152.0 ± 4.8	0.80
Swing time (ms)	115.1 ± 5.3	114.1 ± 4.2	0.93	109.8 ± 4.3	112.1 ± 6.1	0.64
Break time (ms)	83.9 ± 2.6	83.2 ± 3.4	0.34	89.2 ± 2.8	91.2 ± 3.1	0.98
Propulsion (ms)	66.8 ± 6.9	57.6 ± 6.1	0.88	66.5 ± 6.3	66.4 ± 4.0	0.76

Table 1. Data represents mean ± SEM. Control n = 9; *Chrna2*^{Cre};*Viaat*$^{lx/lx}$ n = 8.

JNeurosci Accepted Manuscript

Removal of *Viaat* from the recurrent inhibitory circuit alters motor neuron and Renshaw cell electrical properties.

	Motor Neurons		Renshaw Cells	
	Control	*Chrna2*^{Cre};*Viaat*$^{lx/lx}$	Control	*Chrna2*^{Cre};*Viaat*$^{lx/lx}$
RMP (mV)	-54.9 ± 1.9	-54.6 ± 3.4	-51.6± 0.8	-48.2 ± 1.3 **
Input Resistance (Ω)	119.5 ± 17.4	60.1 ± 5.3 *	282.0 ± 31.2	423.7 ± 36.6 **
Rheobase (pA)	735.4 ± 151.5	1205 ± 315.9	56.1 ± 4.9	39.6 ± 6.7 *
AP Threshold (mV)	-22.2 ± 2.5	-17.3 ± 3.3	-30.3 ± 1.3	-38.4 ± 1.3 ***
AP Amplitude (mV)	54.2 ± 3.3	49.3 ± 4.6	62.5 ± 3.53	64.90 ± 5.31
AP Half-width (ms)	1.2 ± 0.09	1.3 ± 0.1	2.2 ± 0.2	3.0 ± 0.3 *
AHP Amplitude (mV)	-5.9 ± 1.4	-5.7 ± 1.0	-9.4 ± 0.8	-9.4 ± 0.7
Location of peak (ms)	134.6 ± 10.0	97.2 ± 3.8 *	148.8 ± 2.5	159.1 ± 4.2 *
Onset (ms)	97.0 ± 7.3	72.0 ± 2.8 *	127.18 ± 2.1	129.34 ± 1.2
AHP rise (ms)	20.9 ± 1.9	13.6 ± 0.5 *	12.3 ± 0.9	17.8 ± 1.9 **
AHP Half-width (ms)	112.0 ± 12.2	89.0 ± 6.0	63.1 ± 5.7	97.8 ± 13.4 *

Table 2. Data represents mean ± SEM. Motor neuron, control n = 13; *Chrna2*^{Cre};*Viaat*$^{lx/lx}$ n = 9. Renshaw cells, control n = 13; *Chrna2*^{Cre};*Viaat*$^{lx/lx}$ n = 13. * P ≤ 0.05; ** P ≤ 0.01; *** P ≤ 0.001.